ПЛОВДИВСКИ УНИВЕРСИТЕТ
„ПАИСИЙ ХИЛЕНДАРСКИ“

НАУЧНИ ТРУДОВЕ

том 35, кн. 5, 2007

Химия

университетско издателство
Паисий Хилендарски

UNIVERSITY OF PLOVDIV „PAISII HILENDARSKI“ – BULGARIA
SCIENTIFIC PAPERS – CHEMISTRY
VOL. 35, BOOK 5, 2007

ISSN 0204-5346

СЪДЪРЖАНИЕ

ПЛОВДИВСКИ УНИВЕРСИТЕТ „ПАИСИЙ ХИЛЕНДАРСКИ“ – БЪЛГАРИЯ
НАУЧНИ ТРУДОВЕ, ТОМ 35, КН. 5, 2007 – ХИМИЯ
UNIVERSITY OF PLOVDIV „PAISII HILENDARSKI“ – BULGARIA
SCIENTIFIC PAPERS, VOL. 35, BOOK 5, 2007 – CHEMISTRY

EVALUATION OF THE HEATING VALUE OF BIOMASS FUEL FROM ELEMENTAL COMPOSITION AND INFRARED DATA

K. Varmuza, B. Liebmann, A. Friedl
Vienna University of Technology, Institute of Chemical Engineering
Getreidemarkt 9/166, A-1060 Vienna, Austria,
kvarmuza@email.tuwien.ac.at

ABSTRACT

The heating value of 35 biomass samples (wood, cereals) has been modeled from mass% data for carbon, hydrogen, and nitrogen, as well as from infrared data. Regression models have been obtained by application of a genetic algorithm for variable selection and PLS for creation of models. Standard deviation of prediction errors is typically 0.3 % for models from IR data, and 0.7 % for models from elemental composition data.

Keywords: Fuels, IR, chemometrics, variable selection, PLS regression

INTRODUCTION

Biomass is becoming increasingly important as a renewable source of energy, by incineration as well as production of liquid biofuels, e. g. biodiesel or bioethanol. Compared to the incineration of fossil fuels the overall CO_2 balance is considerably less affected by the usage of biomass. Typical biomass materials used for energy production are wood and so-called energy grass. Special types of cereals have a century old tradition in (bio-)alcohol production, recent developments also consider cereal incineration.

An important property of a fuel is its heating value. The so called "higher heating value" (*HHV*) is the enthalpy of complete combustion of a fuel with all carbon converted to CO_2, and all hydrogen converted to H_2O. The higher heating value is given for standard conditions (101.3 kPa, 25 ^oC) of all products and includes the condensation enthalpy of water; it is generally used in the USA. In European countries the "lower heating value" - not used in this study - is more common. It does not include the condensation enthalpy of water [1].

Direct determination of the heating value requires time-consuming calorimetric experiments, which hardly can be automated. Empirical equations have been

published that relate the heating value of a fuel to its elemental composition. Elemental analysis requires tedious laboratory work too, but can be automated. Early mathematical models for coal date back to the late 19th century. Recently, modern chemometric methods have been applied for prediction of heating values of plant biomass from elemental composition [2].

Infrared spectroscopy (IR) and especially near infrared spectroscopy (NIR) became important and routinely used methods for quantitative analyses and for characterization and classification of technological materials and food. IR and NIR can be applied much easier and faster than many other laboratory methods. Chemometric methods allow the generation of multivariate regression models with optimum prediction performance, most used is partial least-squares regression (PLS) [3,4]. Moisture, ash, and heating value have been modeled from NIR data for fuel mixtures of coal, peat, and biofuel [5].

The aim of this study was the development of PLS calibration models for the prediction of higher heating values of wood samples and five different cereals, based on IR reflectance data, and for comparison also on elemental composition data.

EXPERIMENTAL

Samples. A total of n = 35 samples was available, 20 from wood, 15 from cereals. The wood samples consist of sawdust (spruce, pine and larch) with varying amounts of additives such as bark, rye and maize flour, and starch. Cereal samples are unmixed wheat, rye, barley, maize and triticale flours.

Calorimetry. The higher heating value of biomass, *HHV*, has been determined by the bomb calorimetric method according to DIN 51900 T3 [2]. About 1 g biomass material was used; range of measured *HHV* was 18,143 to 19,125 kJ/kg; typical analysis errors are ±60 kJ/kg (ca 0.32 %). The experimental *HHV* values are used as the dependent variable y for regression.

Elemental analysis. The contents of C, H, and N in a sample have been measured by standard methods of elemental analysis as described in a previous work [2]. The concentrations are given in mass% of dry material and have been used as basic x-variables for regression.

Infrared spectroscopy. Spectra were recorded using a Bruker Equinox 55 Fourier Transform-Infrared (FTIR) spectrophotometer equipped with an Attenuated Total Reflection (ATR) accessory and a deuterated triglycine sulfate (DTGS) detector. ATR spectroscopy is a contact sampling method in which a crystal of a high refractive index is used as an internal reflection element. The IR spectra in the range of 4000-600 cm^{-1} were obtained at intervals of approximate 2 cm^{-1} giving 1764 data points per spectrum. Preprocessing of spectra was performed by software Unscrambler [6]: first step was averaging four neighboring absorbance values giving an approximate resolution of 8 cm^{-1}; second step was calculation of the first derivative by the Savitzky-Golay algorithm (quadratic polynomial, three points). The resulting 439 values are used as x-variables in regression.

CHEMOMETRICS

A linear equation that predicts a dependent variable as a function of several independent variables is of the general form

$$\hat{y} = b_0 + b_1 x_1 + b_2 x_2 + b_3 x_3 + \ldots + b_p x_p \qquad (1)$$

where $\hat{y}$ is the predicted dependent variable (*HHV*), b_0 the intercept, b_1 to b_p are the regression coefficients, and x_1 to x_p the independent variables; p is the number of independent variables. PLS regression [3,4] - as implemented in software Unscrambler [6] - has been used for the development of such models. The objective is a model with high prediction performance for cases not used in model building and model optimization. In this study a repeated cross validation (CV) has been applied for optimization of models and estimation of prediction errors. Because of the rather small number of samples available, independent test sets have not been used. The optimum number of PLS components, a_{PLS}, has been determined by a leave-a-quarter-out CV (four segments). From the CV-predicted values ${}_{CV}y_i$ ($i = 1 \ldots n$) the standard error of prediction for CV, SEP_{CV}, has been calculated [3,4,7].

$$SEP_{CV} = [\, \Sigma(y_i - {}_{CV}\hat{y}_i - bias)^2 / (n - 1) \,]^{0.5} \qquad i = 1 \ldots n \qquad (2)$$

The *bias* is the arithmetic mean of the prediction errors ($y_i - {}_{CV}\hat{y}_i$) which in all cases was near zero. *SEP* is identical with the standard deviation of the prediction errors. Four different random splits into four segments have been evaluated and the obtained values for SEP_{CV} averaged; this mean, SEP_{CV4} , is used as a criterion for the prediction performance. In the case of normally distributed prediction errors (which was approximately fulfilled with the used data) $\pm 2.5\ SEP_{CV4}$ is a reasonable confidence interval.

For the elemental analysis data, the basic variable set consists of three variables (mass% of C, H, and N). An augmented variable set has been created by adding nonlinear transformations and combinations of the variables, defined by C^2, H^2, N^2, C·H, C/H, ln(C), ln(H), ln(N), ln(C·H), and ln(C/H), resulting in $p = 13$ variables. Because the added variables are only mathematically defined, a variable selection has been performed using a genetic algorithm (GA, see below) resulting in a variable set with $p = 5$.

For IR data the original variable set consists of 439 variables. Application of a genetic algorithm (GA, see below) resulted in a variable set with $p = 21$.

The principles of genetic algorithms (GA) and successful applications to variable selection have been described by others [8,9]. The software used was MobyDigs [10]. The regression method applied in this software is ordinary least squares regression (OLS) and the performance (fitness) of models has been evaluated by the adjusted correlation coefficient [11] between experimental *HHV* and predicted *HHV* using full cross validation (leave-one-out). The adjusted correlation coefficient considers the number of variables used for the model and penalized models with a large number of variables. Population size used was 50, the maximum number of selected features in a model is limited to 15 by the software. The variables selected in the best 10 best models have been considered. In each trial about 650,000 models were tested. Computation time was 15 minutes for the augmented elemental data set ($p = 13$) and 35 minutes for the IR data set ($p = 439$) on a Pentium 2 GHz.

RESULTS

The heating values, *HHV*, of cereal samples are in the range 18,143 to 18,594 (mean 18,389); all wood samples have higher *HHV*, with a range of 18,668 to 19,125, and a mean of 18,915. The content of carbon shows the same trend with smaller values for cereals (range 40.4 to 42.2%, mean 41.3) than for wood samples (range 46.3 to 47.9%, mean 47.4). Hydrogen and nitrogen contents are higher in cereal samples than in wood samples (H: cereals 6.5 to 6.9%, wood 5.9 to 6.3%; N: cereals 0.9 to 2.2, wood 0.1 to 0.3%).

Figure 1 shows IR spectra from a maize sample and a wood sample. The spectra look very similar and show typical absorptions bands, for instance at about 1000 cm^{-1} from C-OH, at about 1640 cm^{-1} from C=O, and at about 2920 cm^{-1} from C-H; the broad band around 3300 cm^{-1} is from free OH (moisture).

The result of exploratory data analysis by principal component analysis (PCA) is shown in Figure 2. For both data sets a clear separation of the cereals from the wood samples appear. The loading plot for the element data (not shown) reflects the different concentrations of C, H, and N in the two sample groups. The same clustering appears in a dendrogram obtained by hierarchical cluster analysis.

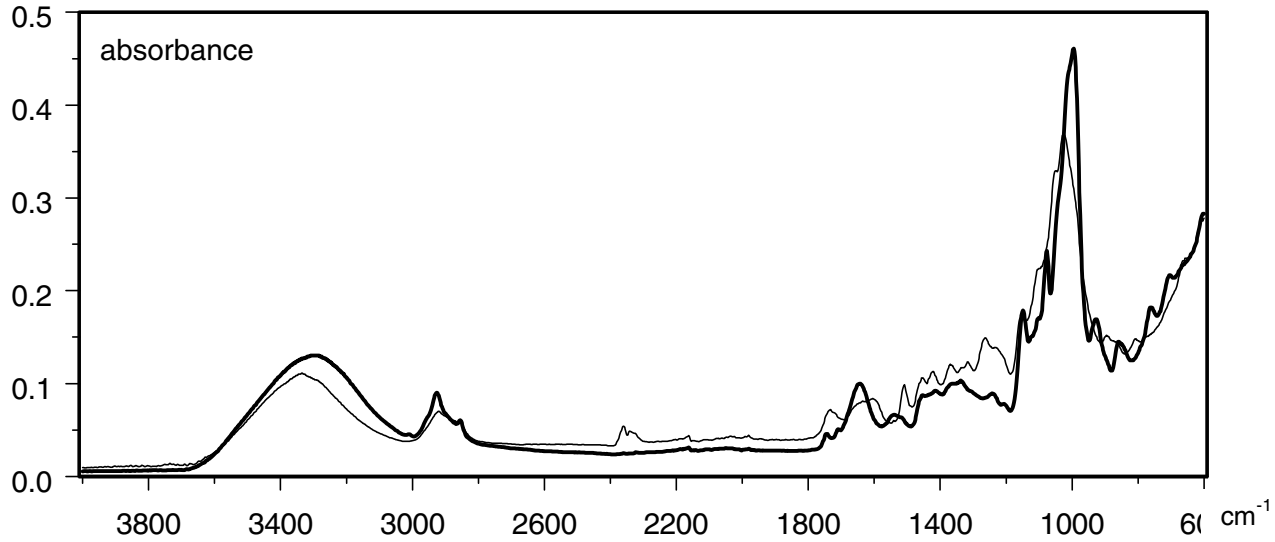

Figure 1. *ATR-FTIR spectra of maize (thick line) and sawdust (spruce) with 18 % bark (thin line).*

Table 1. *Cross-validated PLS models for the higher heating value of biomass derived from elemental composition and infrared data, respectively. p, number of features; a_{PLS}, number of PLS components (averaged); SEP_{CV4}, standard error of prediction (average of four runs of 4-fold cross validation).*

p	Features	Methods	a_{PLS}	SEP_{CV4} *(kJ/kg)*
3	C, H, N	PLS	2	130
13	C, H, N, and derived features	PLS	2	127
5	C, H^2, C·H, C/H, ln(H)	GA + PLS	2	124
439	all IR absorbances	PLS	4	125
21	selected IR absorbances	GA + PLS	12	62

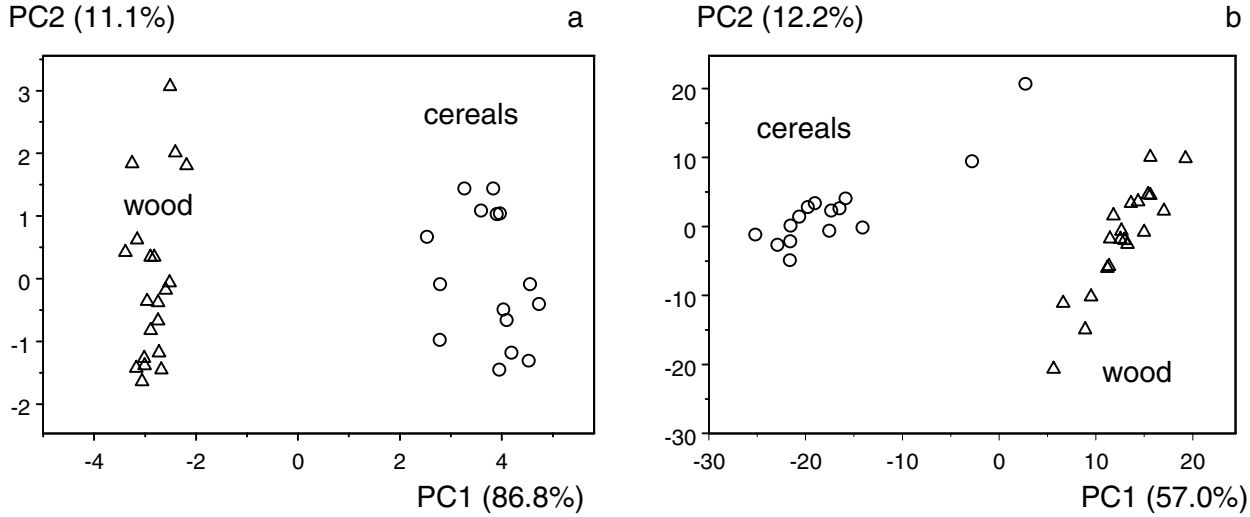

Figure 2. *Principal Component Analysis (PCA) of (a) elemental analysis data (p = 13), and (b) IR data (p = 439) using autoscaled variables, with % preserved variances of first and second principal component scores.*

Modeling the *HHV* by only using the carbon content (univariate regression) gives a standard prediction error, SEP_{CV4}, of 132 kJ/kg. Using the three basic variables from the elemental data (%C, %H, %N) gives 130 kJ/kg. Only a non significant improvement is achieved for the augmented variables set (p = 13) with a SEP_{CV4} of 127 kJ/kg. The variable set from GA selection with p = 5 gives a further small improvement with a SEP_{CV4} of 124 kJ/kg. The best model from elemental data has a standard prediction error of about 0.7 % of the mean of the *HHV* values (Table 1).

A model using all 439 IR variables has a similar prediction performance as models with elemental data with a SEP_{CV4} of 125 kJ/kg. However variable selection by GA resulted in a subset with 21 variables that gives a much better model with a SEP_{CV4} of only 62 kJ/kg. This standard prediction error corresponds to 0.3 % of the mean of the *HHV* values and to a confidence interval of about ±155 kJ/kg. In Figure 3 experimental *HHV* values are plotted versus predicted values obtained from the best model using 21 IR absorbances; the squared Pearson correlation coefficient between calorimetric determined *HHV* and IR-predicted *HHV* is 0.968.

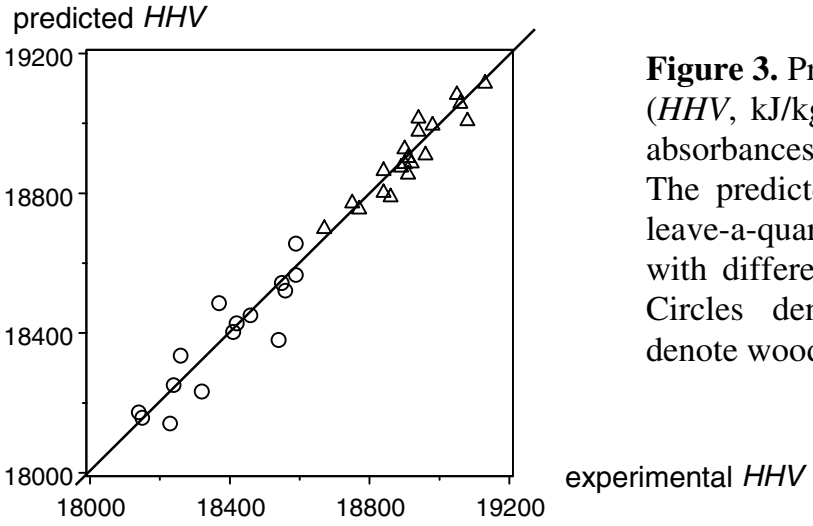

Figure 3. Prediction of higher heating values (*HHV*, kJ/kg) by a PLS model using 21 IR absorbances selected by a genetic algorithm. The predicted values are means from four leave-a-quarter-out cross validation runs with different partitioning of the segments. Circles denote cereal samples, triangles denote wood samples.

CONCLUSIONS

Easily available IR reflection data are promising for the determination of heating values of wood and cereal samples. Feature selection by a genetic algorithm improved the prediction performance in comparison to models with all features. IR data are better suited than elemental composition data. A single model can be used for wood samples and cereal samples.

Acknowledgements. We gratefully acknowledge financial support by Hochschuljubiläumsstiftung der Stadt Wien, Projekt H-7022005. We thank A. Kandelbauer from Competence Center Wood K-Plus (St. Veit an der Glan, Austria) for instrumental support, E. Padouvas for calorimetric measurements, and H. Mikosch for IR support (both Vienna University of Technology), and H. Schausberger (Saatbau Linz, Austria) for providing cereal samples.

REFERENCES

[1] Corbitt, R. A., Standard handbook of environmental engineering. Mc Graw Hill, New York, 1989.
[2] Friedl, A., Padouvas, E., Rotter, H., Varmuza, K., Anal. Chim. Acta 544 (2005) 191-198.
[3] Naes, T., Isaksson, T., Fearn, T., Davies, T., A user-friendly guide to multivariate calibration and classification. NIR Publications, Chichester, 2004.
[4] Varmuza, K., in: Gasteiger, J. (Eds.), Handbook of chemoinformatics, Vol. 3, Wiley-VCH, Weinheim, 2003, p. 1098-1133.
[5] Geladi, P., Lillhonga, T., Reuter, L., in: Pomerantsev, A. L. (Ed.), Progress in chemometrics research, Nova Science Publishers, New York, 2005, p. 193-208.
[6] Camo Process AS, Software The Unscrambler. http: //www.camo.no, Oslo, Norway, 2002.
[7] Kramer, R., Chemometric techniques for quantitative analysis. Marcel Dekker, New York, 1998.
[8] Forina, M., Lanteri, S., Oliveros, M. C. C., Millan, C. P., Anal. Bioanal. Chem. 380 (2004) 397-418.
[9] Leardi, R., Boggia, R., Terrile, M., J. Chemometrics 6 (1992) 267-281.
[10] MobyDigs, 1.0. Talete srl, www.talete.mi.it, Milan, Italy, 2004.
[11] Frank, I. E., Todeschini, R., The data analysis handbook. Elsevier, Amsterdam, 1994.

ПЛОВДИВСКИ УНИВЕРСИТЕТ „ПАИСИЙ ХИЛЕНДАРСКИ“ – БЪЛГАРИЯ
НАУЧНИ ТРУДОВЕ, ТОМ 35, КН. 5, 2007 – ХИМИЯ
UNIVERSITY OF PLOVDIV „PAISII HILENDARSKI“ – BULGARIA
SCIENTIFIC PAPERS, VOL. 35, BOOK 5, 2007 – CHEMISTRY

BIOCATALYSTS – PRODUCTION AND APPLICATION

Ivan Pishtiyski
Department of Biochemistry and Molecular Biology, University of Food Technologies, 26 Maritza Blvd., 4000 Plovdiv, Bulgaria, E-mail:ivgenpy@gmail.com

ABSTRACT

A short review of the stages of enzymology development is presented in the paper. The processes for producing enzymes with different purity are presented schematically. The possibilities for their application in different arias of industry are considered. Particular examples with the enzymes pectinesterase, cyclodextrin glucanotransferase, lipase, etc. are presented.

Keywords: biocatalysts, production, application, cyclodextrin glucanotransferase, lipase

Two centuries from the discovery of the first enzyme diastase (amylase) in 1814 by the russian scientist Konstantin Sigimundovich Kirhoff will be fulfilled in several years [11]. His discovery was a result from the research on the problem with the sugar insufficiency in Russia in the beginning of the nineteenth century, which occurred as a result of the slaves rising in the sugar plantations and Napoleon blockade. The progress in the research in the biocatalysis processes raised the questions if the biocatalysis reactions are a variety of the chemical reactions, if the chemical rules are valid, if the chemical methods are suitable for investigation of the biochemical reactions.

The answering of these questions has taken more than a century and was connected with plenty of methodological difficulties. The history of the enzymology can be divided into the following stages:

- Production of the first enzyme preparations (1814-1860);
- Beginning of the simultaneous investigation on the biocatalysts and the biochemical processes (1860-1890);
- Research on the specificity of the enzyme action (1894-1920) [8];
- Isolation, purification; and determination of the enzymes composition and their action mechanism (1920-) [23,29];

- Investigation on cofactors, development of the concept for the enzyme two components nature and for the cofactoring functions vitamins (1920-1940);
- Application of the enzymes in different spheres of industry (1910-) [1,26];
- Preparation and application of immobilized enzymes (1914-) [10,12,28,30,].

The discoverer of the enzymes Konstantin Kirhoff could hardly imagine that he put the beginning of a whole field of science, which would allow processes intensifications, their performance at extremely mild conditions, environment protection, production of ecology clean and high quality products, performance of high precise analysis, etc.

When preparing this review, I have established that biocatalysis was a subject of a great deal of investigations. Over 40000 titles appeared only in the period 2001-2006. Summarizing this scientific wealthy is a rather complex task. Without having any claims for comprehensiveness and thoroughness**,** I will try to present a part of the achievements in this area in combination with some of the researches in the department, where I work, focusing on the biocatalysis application. Prior to the discussion of the theme, I will accentuate on the production of enzyme preparations [4,13].

The scheme on Figure 1 gives a brief summary of the production of different types of enzyme preparations. The first stage is the choice of an appropriate enzyme source. There are three possibilities: plant, animal, and microbial sources. The first two sources are limited, since the raw material is insufficient (for the animal enzymes), and the content of the enzyme in the plant materials is rather low, which necessitates processing of a great amount of raw material at low yield. Basic source for enzyme production is microorganisms, which possess the following advantages:

- A great number of enzymes with various properties;
- Possibilities for application of genetic methods, which leads to yield increase of the enzyme produced [25];
- High growth rate of the cells;
- Secretion of the enzymes in the culture liquid, which enables easy isolation.

Depending on the application, enzymes preparations with different degree of purity can be produced, which affects their final price. The most simple scheme is the production of crude enzymes (variant I). More complicated is the scheme for production of purified enzymes (variant II and III), and the most complicated method is for the homogenic ones (variant IV) [9].

The possibilities for enzymes applications are comprehensive (Figure 2). The broadest application is in the food and flavor industry. The most widely used sweet substance in every day life is sugar, which is produced from sugar beet and sugar-cane. However, corn could be also used for raw material. “Liquid sugar” with 60 % higher effectiveness in comparison to the traditional sources could be produced from corn starch by the means of several enzymes: α-amylase, glucoamylase, glucoseisomerase, pulullanase, etc [18]. The world production of this product is about 30-35 % in comparison to the total amount of sugar consumed [19,24].

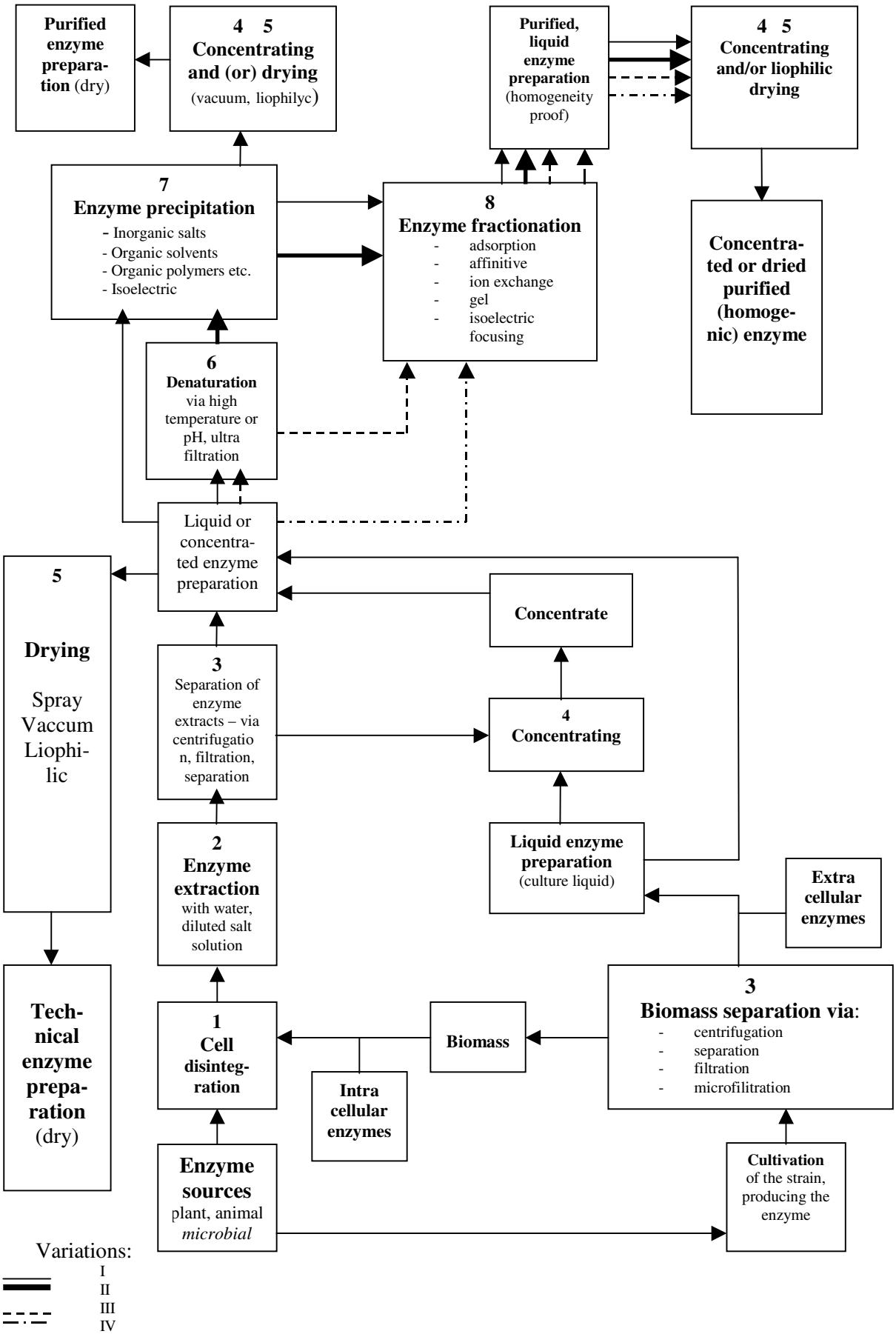

Figure 1. *Scheme for isolation and purification of enzyme preparation*

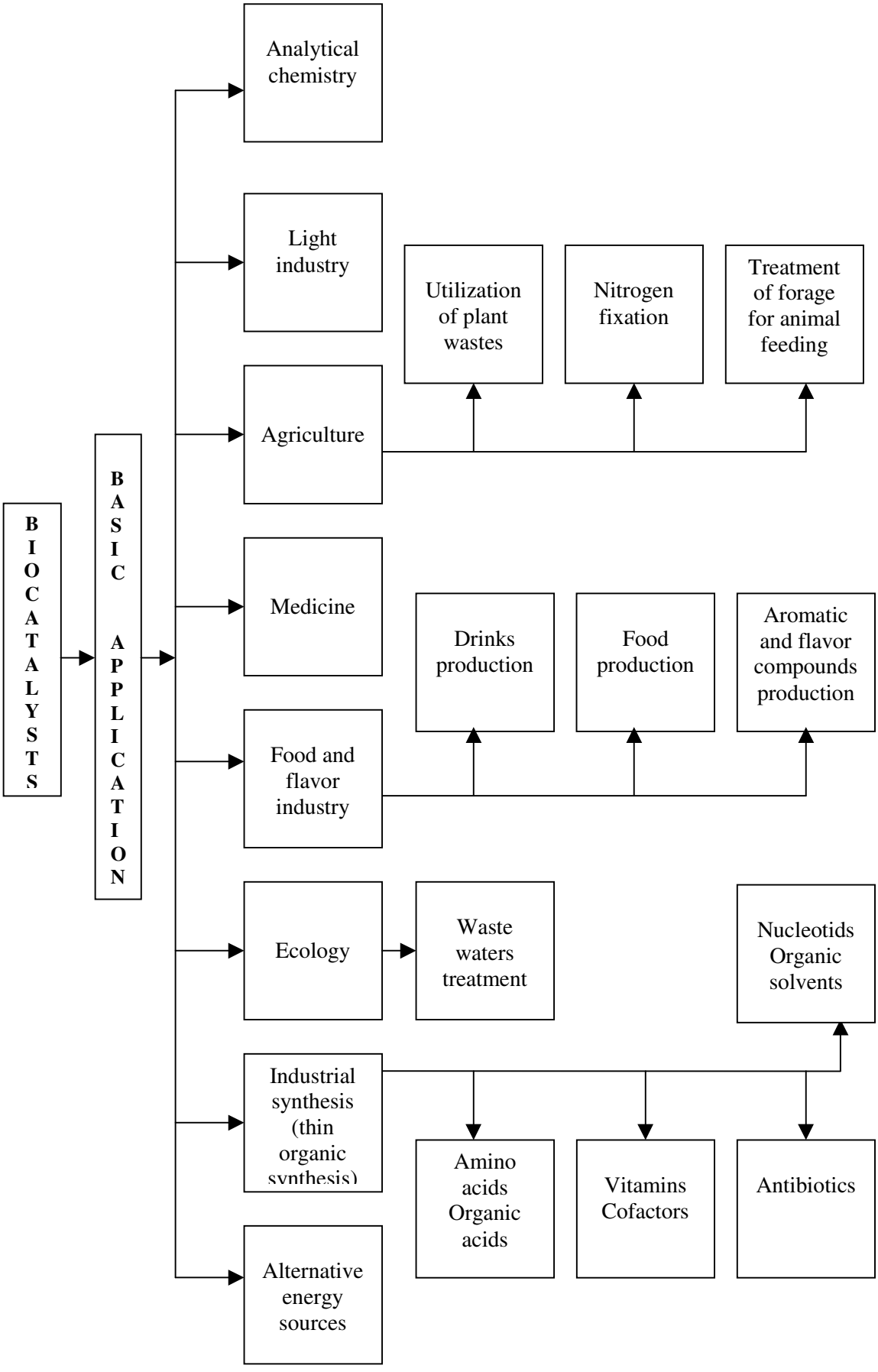

Figure 2. *Enzyme applications*

The liquid sugar is preferred for many food products. In our country this production is performed by Amylum-Razgrad. The glucose-fructose syrup is only a part of their products. Liquid and dry glucose, high inverted syrups, suitable for brewery and alcoholic industry, are also produced by the means of enzyme hydrolysis. The advantages of these technologies are as following: environment friendly, complete utilization of the raw material, high conversion degree of starch (over 95 %). For these reasons amylases comprise about 30 % of the commercially produced enzymes [24]. Strains have been selected, which produce thermostable α-amylases, useful at starch claysterization (100-110°C) and liquefaction (80-90°C) [2,5,6,18,20,21,27].

The taste of the dairy products (different cheese) is well known for everybody. Their production is an example of fine biocatalysis action. It is enough only one peptide bond from the stable casein molecule from the milk to be degraded in order to unstabilize it. The milk protein begins to precipitate, the precipitate formed aggregates gradually, and the valuable milk products are formed as a result of additional biochemical processes. The tool for this transformation is the enzyme rennin. In order to answer the increased demand of the dairy products, it was necessary to find a substitute of the naturally produced enzyme from young animals. Such microbial enzymes have been already produced and their properties are very close to the natural enzyme, which guaranties a high quality of the dairy products.

Bread is a food product, which we use every day. The production of high quality bread requires a great skill of the bakers. Nowadays, science is helping them. Different additives, for the bread industry have been made. They allow improvement of the bread consistence, and aroma. These additives constitute of enzymes such as α-amylase, xylanase, and glucoamylase [3,7]. Their action enables formation of greater amount fermentable sugars, higher content of CO_2, which is hold back in the dough, leading to increased bread volume, and improved texture. Together, the Meyer reaction is accelerated, and the content of the aroma substances is increased.

The examples could be proceeded, but I will focus on the ones, which are a subject of research in the department of Biochemistry and molecular biology, UFT.

The first one is connected with the enzyme pectinesterase. It hidrolyses the ester bonds of methanol in the pectin molecule, reducing the esterification degree. As a result moderate or low esterificated pectins are formed. They have altered properties and are valuable additives for pectin containing products, improving their nutrient and biological characteristic. The enzyme pectinesterase is not produced pure. It is in a complex with other pectolytic enzymes, which degrade pectin molecule. The separation of this complex is almost impossible procedure, even using chromatographic methods. We have succeeded to work out an easy method, connected with the change of pH of the enzyme solution, resulting in an isolation of a pure pectinesterase [14]. This allowed us to perform a controllable biochemical process for deesterification of pectin at mild conditions and to produce pectins with desirable esterification degree [15,16,17]. The production of this enzyme is performed in the enzyme factory in Botevgrad. Unfortunately pectin production in our country is at standstill in recent years, and the use of the enzyme is stopped.

The other example is connected with the enzyme cyclodextrin glucanotransferase, which is produced only by microorganisms, mainly bacteria. Extremely valuable compounds – cyclodextrins (CD) are formed by the means of the enzyme. They are starch derivatives, cycling molecules consisting of 6, 7 or 8 glucose units, called respectively α-, β-, and γ-CD (Figure 3).

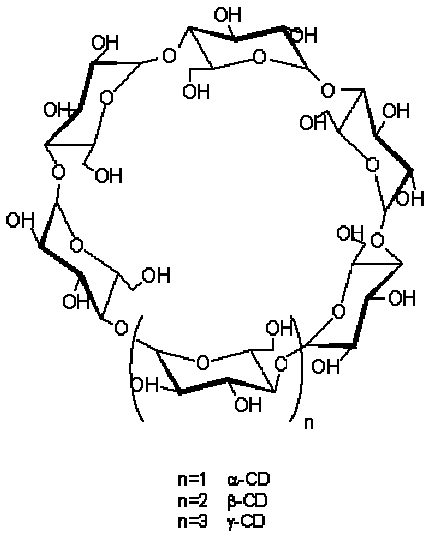

Figure 3. *Cyclodextrin view*

In their molecule a cavity is formed, in which different compounds – vitamins, aroma substances, lipids, drug formulations, pesticides, microelements can be situated. As a result complexes are formed, in which the guest molecules are with increased stability towards hydrolysis, oxidation, dehidratation, evaporation, thermal treatment, etc. The complexes gain valuable specific properties, which enable the nutrition and biological properties of food products to be preserved for a long time, the pharmaceutical and pharmacological characteristics of drugs to be improved by prolonged action of the active compound. For these reasons CD are applied in food and flavor industry, medicine, biotechnology, cosmetics, agriculture, etc.

One of our projects is about biosynthesis and characterization of this enzyme. The optimal nutrient medium composition and cultivation conditions for maximal enzyme amount have been established. Some of its properties were also determined (Figure 4).

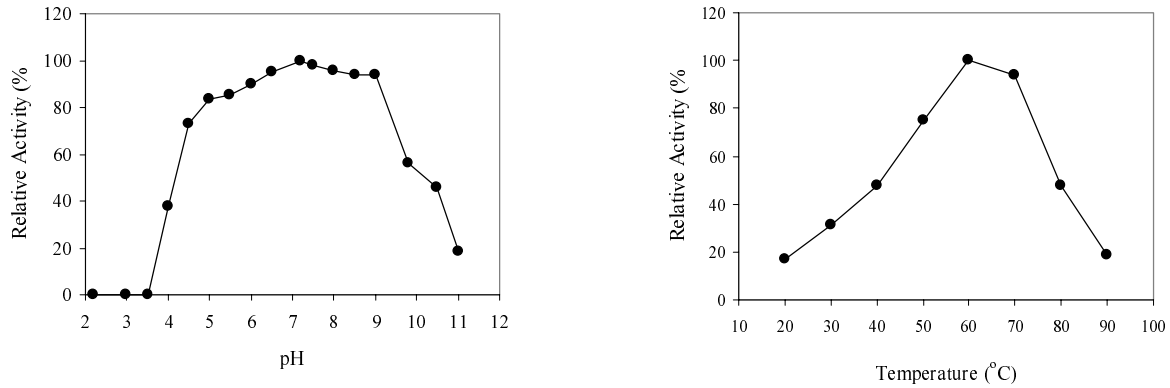

Figure 4. *Effect of pH and temperature on purified CGTase activity (pH 7.5)*

The possibilities for CD production with the isolated enzyme have been investigated in another research. Interesting results have been registered, which presume high starch conversion degree in CD (Table 1).

Table 1. *Effect of reaction time on CD yield*

№	Time, h	CGTase 1 U/g		CGTase 2 U/g			CGTase 4 U/g		
		YIELD*, %							
		With shaking	Without shaking	With shaking	Without shaking		With shaking	Without shaking	
		With toluene		With toluene		Without toluene	With toluene		Without toluene
1	1	14.75	12.62	18.20	20.70	16.84	18.68	28.41	27.32
2	2	21.93	21.26	22.27	28.55	24.85	26.60	42.77	33.96
3	3	25.32	23.62	27.65	35.77	26.07	43.45	54.97	35.72
4	4	37.00	33.70	40.30	44.60	29.79	53.63	56.90	35.96
5	5	40.62	34.72	46.71	51.20	31.29	57.90	59.47	38.60
6	8	42.68	40.28	51.94	56.90	31.43	63.41	65.01	39.07
7	24	48.80	49.28	56.31	59.90	33.82	69.50	71.91	40.97
8	24**	41.62	46.85	45.75	50.43	29.56	51.05	53.92	30.02

5 % starch solution; 40°C; pH – 6.0; * Reaction mixture is used for analysis; ** Analysis of isolated CD

The investigations in the last decade have shown that enzymes and whole cells can be successfully used in the organic synthesis. The enzymes are most often applied in hydrolysis and isomerisation reactions, and the whole cells are used in synthesis reactions, in which the cofactors should be regenerated. This is easier in vivo than in vitro.

One of enzymes advantages is their extreme specificity, selectivity. It enables their use as valuable catalysts in the production of biologically active compounds with chyral centers or position isomers. They allow simple or complicated transformations to be performed without the use of blocking and deblocking steps, characteristical for the organic synthesis. Another advantage of the enzymes is that by-products are not formed.

Some of the products produced enzymaticaly at several well known chemical companies are presented in Table 2 [22].

The use of the enzymes in organic synthesis has become possible as a result of the explanation of the enzymes action mechanism. As an example I will consider the enzyme lipase. It degrades the ester bonds between the fatty acids and alcohols or polyalcohols. The group of lipases consists of a great number of enzymes, which catalyses different ester bonds, i. e. they do not have a high specificity. The active site of lipases contains the amino acids serine, histidine, aspartic or glutamic acid. The hydrolysis of the ester bonds involves formation of acid-enzyme complex (Figure 5). The biocatalysis process begins with nucleophilic attack of serine OH group towards the carbon atom of COOH group of the ester bond. The complex is degraded via nucleophilic attack of water, the fatty acid is released and the enzyme is restored.

Table 2. *Biocatalytic systems at several chemical companies*

Product	Substrate	Reaction	Enzyme	Scale, ton/year	Yield	Source
Amides, alcohols, acids						
Enantiopure alcohols	Racemic alcohols	Resolution	Lipases	Thousand	Excellent	BASF
R-amide; S-amine	Racemic amines	Resolution	Lipases	Hundreds	Excellent	BASF
R-mandelic acid	Racemic mandelonitrile	Hydrolysis	Nitrilases	Several	Excellent	BASF
Amino acids, penicillins						
Non-proteinogenic L-amino acids	Racemic aminoacid amides	Kinetic resolution	Amidases	Several hundred		DSM
L-Aspartic acid	Fumaric acid	Addition of ammonia	Aspartic acid liase	Thousand		DSM
Aspartame	L-Aspartic acid phenylalanine Methyl ester	Selective coupling	Thermo-lisine	Thousand		DSM
6-APA	Penicillin G/V	Hydrolysis	Penicillin acylase	Thousand		DSM
Semisynthetic penicillins	6-APA	Selective coupling	Acylases	Several hundred		DSM
N-heterocyclic compounds						
6-Hydroxy nicotinic acid	Niacin	Addition of water	Niacin xydroxylase	Few	65 g/l	Lonza
6-Hydroxypirazine carboxylic acid	2-Cyanopyrazine	Addition of water	Nitrilase/ xydroxylase	Development product	40 g/l	Lonza
6-Hydroxy-5-nicotine	5-Nicotine	Addition of water	xydroxylase	Development product	30 g/l	Lonza

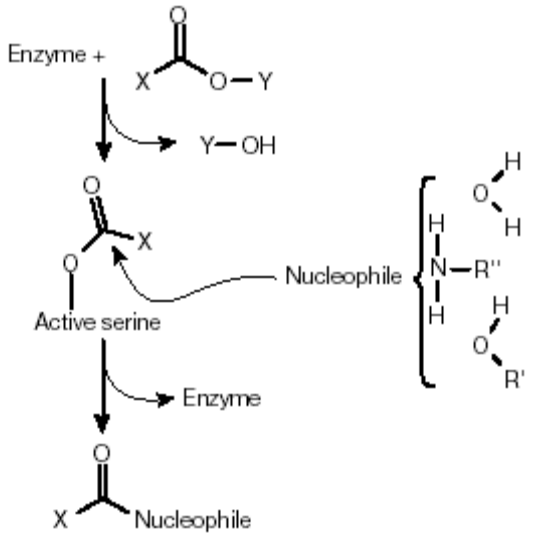

Figure 5. *Reaction mechanism of lipase biocatalysis*

As lipases are also active in organic solvents, water can be substituted by another nucleophile, alcohols for example. As a result preesterification or transesterification proceeds. Only the one isomer (enantiomer) from racemic mixtures can be acylated, which leads to selective transformation. Suitable acidic donors are

vynile esters, anhydrides or diketones. The reaction is non convertible and the unused alcohol and the ester produced are easily separated. This approach is used for production of pure enantiomeric alcohols. Amines could be also nucleophiles, which allows racemic amines to be separated. Characteristic for this approach is the high yield, selectivity and the minimal enzyme amount needed.

These are only a small part of the enzyme processes applied in the production of organic compounds, including biologically active substances. Their amounts are in the range of hundreds tons.

REFERENCE

1. Boyce, C. 1984. Developing a new industrial enzyme application: A strategy. J Oil Chem Soc 61, 1750-1753.
2. Canganella, F., Andrade, C., Antranikian, G., 1994. Characterization of amylolyticand pullulytic enzymes from thermophilic archaea and from a new Ferividobacterium species. Appl. Microb. Biotechnol. 42, 239–245.
3. Courtin, C.M. and Delcour, J.A. 2002. Arabinoxylans and endoxylanases in wheat flour bread-making, J.Cer. Sci., 35, 225-243.
4. Cowan, D. 1996. Industrial enzyme technology. Trends Biotechnol. 14 (6), 177-178.
5. Crab, W., Mitchinson, C. 1997. Enzymes involved in the processing of starch to sugars. Trends Biotechnol. 15, 349-352.
6. Demirijan, D., Moris-Varas, F., Cassidy, C. 2001. Enzymes from extremophiles. Curr. Opin. Chem. Bull. 5, 144–151.
7. Durton, A. Georis, J., Genot, B., Dauvrin, T., Collins, T.,Hoyox, A., and Feller, G. Use family 8 enzymes with xylanolytic activity in baking. Patent number WO 2004023879 A1, 2004.
8. Fischer, E. 1909. Untersuchungen uber Kohlenhydrate und Ferments, Bd.I. 1884-1909, Berlin.
9. Gessesse, A. 1998. Purification and properties of two thermostable alkaline xylanases from an alkaliphilic Bacillus sp. Appl. Environ. Microbiol. 64, 3533–3535.
10. Groboillot, A. 1994. Immobilization of cells for application in the food industry. Crit. Rev. Biotechnol. 14, 75–107.
11. Kirchhoff, G.S.C. 1815. Uber die Zuckerbildung beim Malzen des Getreides und beim Bebruhem seines Mehls mit kochendem Wasser. Schweigger.-J.Chem.Phys., 14, 389-398.
12. Krastanov, A. 2000. Removal of phenols from mixtures by co-immobilized laccase/tyrosinase and Polyclar adsorption, J. Ind. Microbiol. Biotech., 24, 1-6.
13. Leuschner, C., Antranikan, G. 1995. Heat stable enzymes from extremely thermophilicand hyperthermophilicmic microorganisms. World J. Microbiol. Biotechnol. 11, 95–114.
14. Ljutzkanov, N., Pishtiyski, I. Method for production of enzyme preparations of pectinesterase. Avtorsko svidetelstvo N 29659/2.06.1981.

15. Ljutzkanov, N., Pishtiyski, I., Koleva, L., Tziporkov, N. Method for deesterification of pectin. Avtorsko svidetelstvo N 38239/01.06.1984.
16. Ljutzkanov, N., Pistijsky I., Influence of pH on deesterification of pectin by microbial pectinesterase, Travaux scientifiques, HIFFI, XXXIII, I, 1986.
17. Pistijsky, I., Ljutzkanov, N., Koleva, L. 1986. Influence of some factors on pectin deesterification by means of microbial pectinesterase, Travaux scientifiques, HIFFI, XXXIII, I.
18. Poonam, N., Dalel, S. 1995. Enzyme and microbial systems involved in starch processing. Enzyme Microb. Technol. 17, 770–778.
19. Rakshit, S.K. 1998. Utilization of starch industry wastes. In: Martin, A. (Ed.), Bioconversion of Waste Materials to Industrial Products, second ed. Blackie Academic and Professional, London.
20. Rudiger, A., Jorgensen, P., Antranikan, G. 1995. Isolation and characterization of a heat stable pullulanase from the hyperthermophilic archeon Pyrococcus woesei after cloning and expression of its gene in Escherichia coli. Appl. Environm. Microbiol. 61, 567–575.
21. Sarikaya, E., Higassa, T., Adachi, M., Mikami, B. 2000. Comparison of degradation abilities of α- and β-amylases on raw starch granules. Proc. Biochem. 35, 711–715.
22. Schmid, A., Dordick, J.S., Hauer, B., Kieners, A., Wubbolts, M., Witholt, B. 2001. Industrial biocatalysis today and tomorrow, Nature, vol.409, 258-268.
23. Vakhlu, J., Kour, A. 2006. Yeast lipases: enzyme purification, biochemical properties and gene cloning, Electronic J Biotechnol. 9 (1), January 15.
24. Van der Maarel, M., Van der Veen, B., Uitdehaag, H., Leemhuis, H., Dijkhuizen, L. 2002. Properties and applications of starchconverting enzymes of the α-amylase family. J. Biotechnol. 94, 137–155.
25. Van der Veen, B., Uitdehaag, J., Penninga, D., Van Alebeek, G., Smith, L., Dijkstra, B., Dijkhuizen, L. 2000. Rational design of cyclodextrin glycosyltransferase from Bacillus circulans strain 251 to increase α-cyclodextrin production, J. Mol. Biol. 296, 1027-1038.
26. Vellard, M. 2003. The enzymes as drug: application of enzymes as pharmaceuticals. Curr Opin Biotechnol 14, 1-7.
27. Viara, N., Elena, P., Elka, I., 1993. Purification and characterization of a thermostable alpha-amylase from *Bacillus licheniformis*. J. Biotechnol. 28, 277–289.
28. Wang, P., Sergeeva, M.V., Lim, L., Dordick, I.S. Biocataliticplasticsasa active and stable materials for biotransformations. Nature Biotechnol. 15, 789-793.
29. Willstatter, R., Bamann, E. Uber die Proteasen der Magenschleihaut. I. Uber Enzyme der Leukozyten. Z physiol.Chem., 180, 127, 1928-1929.
30. Yang, Z. et al. 1995. Activity and stability enzymes incorporated into acrylic polymers. I.Am.Chem.Soc.117, 4843-4850.

ПЛОВДИВСКИ УНИВЕРСИТЕТ „ПАИСИЙ ХИЛЕНДАРСКИ“ – БЪЛГАРИЯ
НАУЧНИ ТРУДОВЕ, ТОМ 35, КН. 5, 2007 – ХИМИЯ
UNIVERSITY OF PLOVDIV „PAISII HILENDARSKI“ – BULGARIA
SCIENTIFIC PAPERS, VOL. 35, BOOK 5, 2007 – CHEMISTRY

Cu-Cr/γ-ALUMINA CATALYSTS FOR DIMETHYL ETHER SYNTHESIS

Dimitar Dimitrov and Krasimir Ivanov
Dept. of Chemistry, Agricultural University – Plovdiv
e-mail: kivanov1@abv.bg

ABSTRACT

The investigation relates to catalysts, comprising copper-chromium spinel, coated on γ-Al_2O_3 carrier. The effect of catalyst composition on the activity behavior toward dimethyl ether synthesis was discussed. It was found that the mixed CuO – Cr_2O_3 catalysts are very active with regard to the methanol dehydration. A synergetic effect of both copper and chromium species is clearly observed.

Keywords: copper-chromium catalysts, dimethyl ether, synthesis

INTRODUCTION

Dimethyl ether (DME) is a multipurpose clean fuel and chemical feedstock that can be produced from a wide variety of sources and has a number of important applications. It is a useful chemical intermediate for the preparation of many important products, such as dimethyl sulfate and high-value oxygenated compounds (1-3). In addition, it has been used as an aerosol propellant to replace chlorofluoro carbons which can destroy the ozone layer of the atmosphere (4). Recently, it has received much attention as an alternative diesel fuel by virtue of its low NO emission, near-zero smoke and less engine noise compared with those of traditional diesel fuels (5, 6).

Commercially, DME is produced by the catalytic dehydration of methanol at around 300^{o}C at 10 atm pressure over solid acid catalysts such as γ-Al_2O_3 or zeolites, combined with different additives (7, 8). The main problems with the catalysts is coke formation and coating of the surface with carbon, which requires their replacing more frequently than is desirable. This necessitates search for new catalysts with high activity and long period of exploitation.

In this paper we have studied the role of the catalyst composition of the alumina supported CuO - Cr_2O_3 in the methanol dehydration process.

MATERIALS AND METHODS

Commercial γ-Al_2O_3 F-2000 with particle size of 4,8 mm and total pore volume of 0,5 sm^3/g was used as a carrier. The catalysts were prepared by impregnation of the support with an aqueous solution of copper and chromium nitrates.

All experiments were carried out on a flow apparatus for estimation of oxide catalysts for methanol oxidation and dehydration, using stainless steel pseudo-isothermal reactor (Fig. 1).

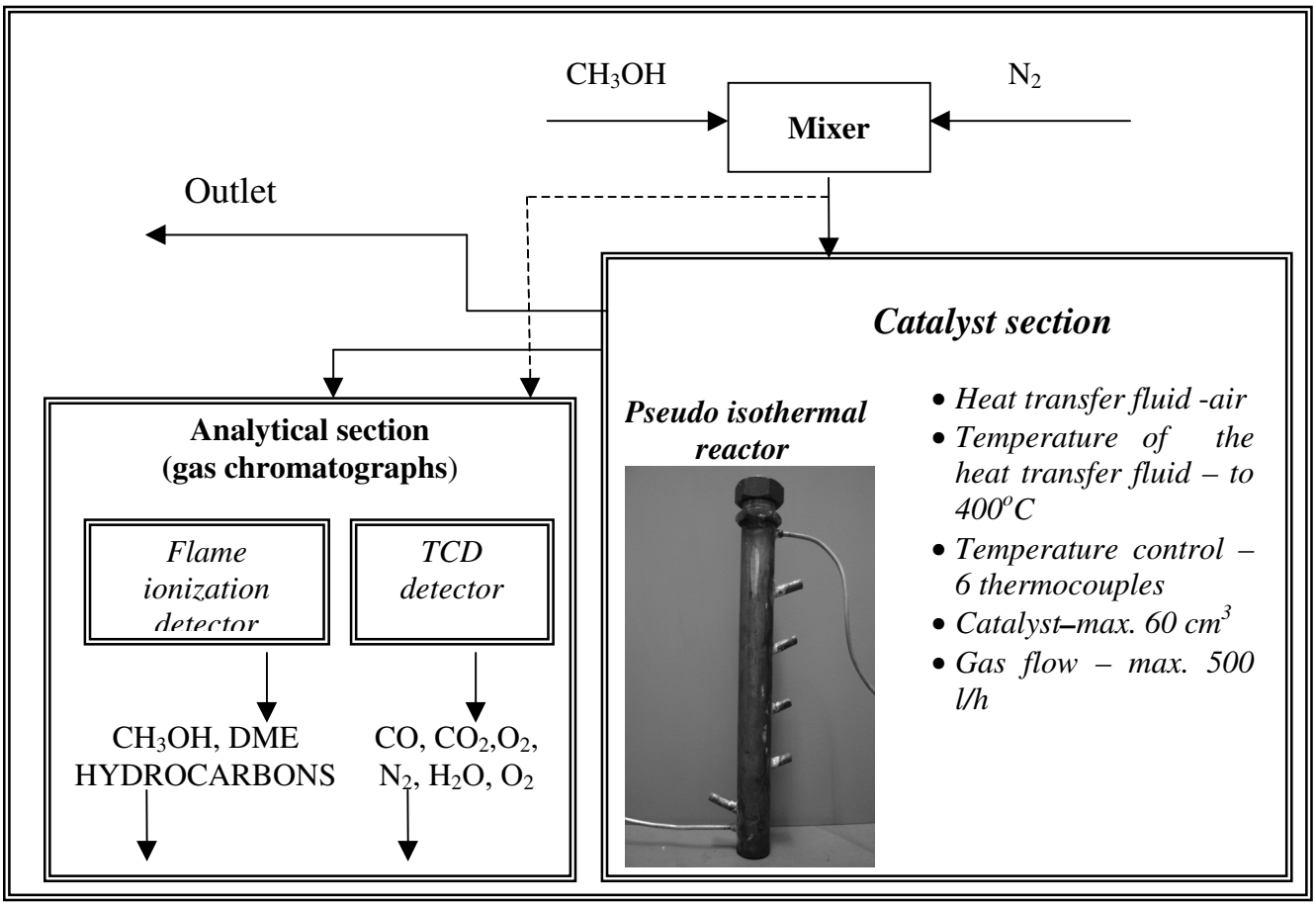

Figure 1. *Apparatus for estimation of oxide catalysts for methanol oxidation and dehydration.*

The outlet gas mixture was analyzed for dimethyl ether (DME), methanol, CO, dimethoximetan (DMM) and hydrocarbons content in the analytical section by on-line gas chromatograph, equipped with flame-ionization detector and Porapak Q column. A second gas chromatograph, equipped with a thermal conductivity detector and MS-13X column was employed for CO determination.

RESULTS AND DISCUSSION

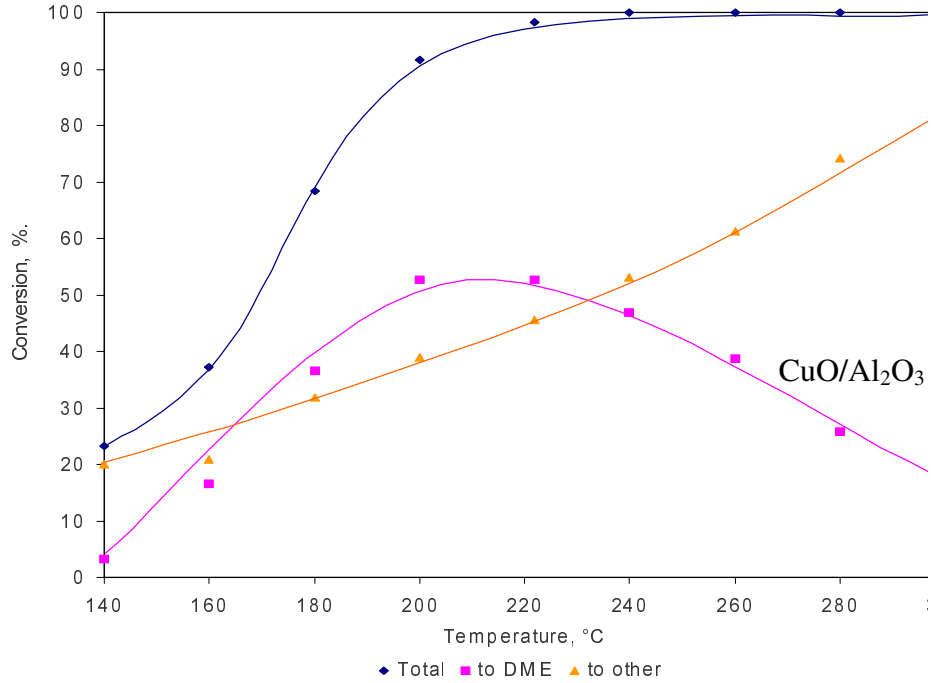

Figure 2. *Product distribution versus temperature. Feed gas composition: methanol 4,0 %, nitrogen to 100 %.*

Table 1. *Product distribution versus temperature. Feed gas composition: methanol 4,0 %, nitrogen to 100 %.*

Temperature, °C	Conversion, %		
	Total	To DME	To other products
300	100,0	16,7	83,3
280	100,0	25,9	74,1
260	100,0	38,6	61,4
240	100,0	46,8	53,2
220	98,3	52,7	45,6
200	91,7	52,7	39,0
180	68,3	36,6	31,8
160	37,3	16,5	20,8
140	23,3	3,2	20,1

Fig. 2 and Table 1 reflect the temperature dependence of methanol conversion on alumina supported copper oxide. As it is seen from the results presented, the activity of the catalysts with regard to the total methanol conversion is significant even at temperatures lower than 200°C. The conversion to DME passes through maximum at 200 – 240°C and rapidly decreases along with the temperature, while

conversion to other products (mainly hydrocarbons) increases in the whole temperature interval.

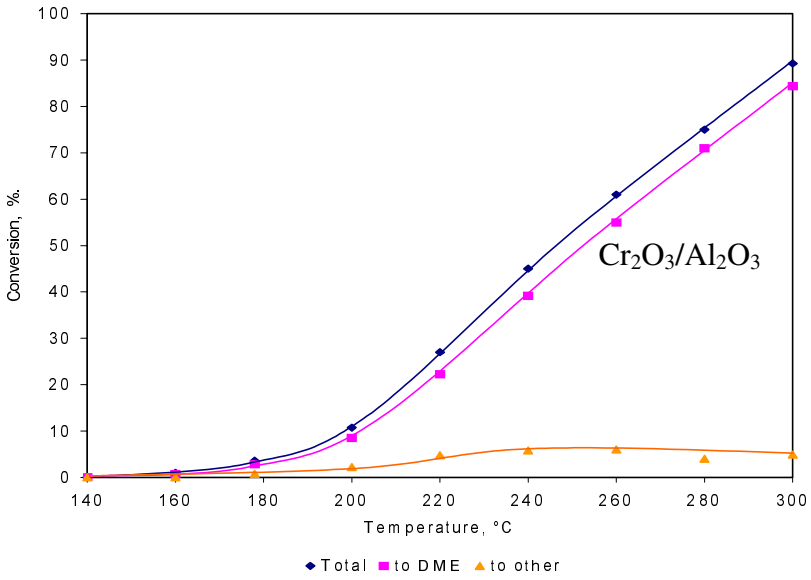

Figure 3. *Product distribution versus temperature. Feed gas composition: methanol 4,0 %, nitrogen to 100 %.*

Table 2. *Product distribution versus temperature. Feed gas composition: methanol 4,0 %, nitrogen to 100 %.*

Temperature, °C	Conversion, %		
	Total	To DME	To other products
300	89,3	84,4	4,9
280	75,0	72,0	3,0
260	61,0	55,0	6,0
240	45,0	39,2	5,8
220	27,0	22,2	4,8
200	10,7	8,5	2,2
180	3,6	2,8	0,7
160	0,0	0,0	0,0
140	0,0	0,0	0,0

Fig. 3 and Table 2 reflect the temperature dependence of methanol conversion on alumina supported chromium oxide. The activity of the alumina supported chromium oxide is vastly lower than that of copper oxide. The reaction starts at only about 180°C, but the selectivity towards DME synthesis is very high even at 300°C.

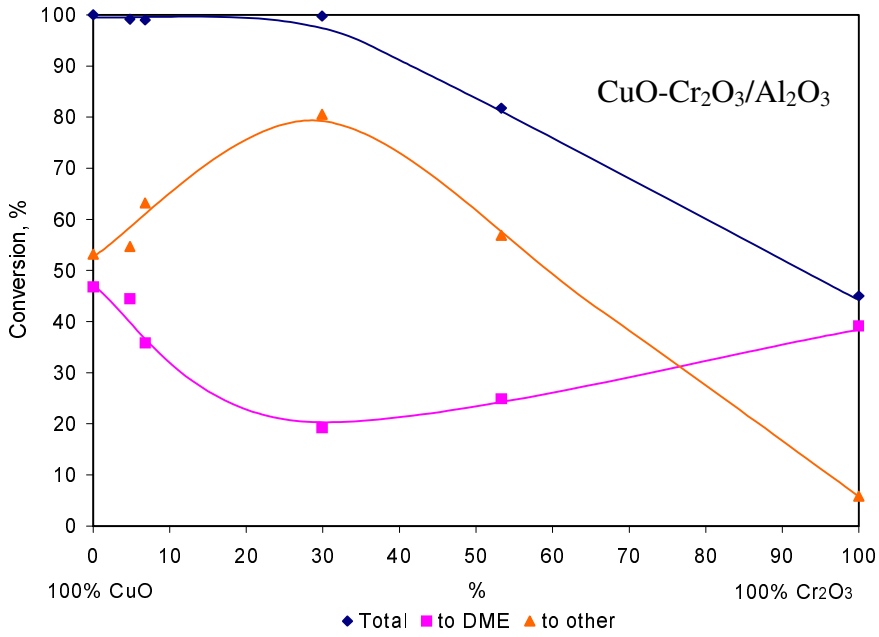

Figure 4. *Product distribution versus catalyst composition at 240°C . Feed gas composition: methanol 4,0 %, nitrogen to 100 %.*

Table 3. *Product distribution versus catalyst composition at 240°C . Feed gas composition: methanol 4,0 %, nitrogen to 100 %.*

Catalyst composition		**Conversion, %**		
Cr_2O_3, %	**CuO, %**	**Total**	**To DME**	**To other products**
0,0	100	100,0	46,8	53,2
4,8	95,2	99,1	44,5	54,7
6,8	93,2	99,0	35,8	63,2
29,9	70,1	99,8	19,2	80,5
53,3	46,7	81,8	24,9	56,8
100,0	0,0	45,0	39,2	5,8

Fig. 4 and 5 and Tables 3 and 4 present the influence of catalyst composition on methanol conversion and product distribution at 240 and 300°C. The tendencies at both temperatures are identical. The total conversion of methanol decreases as Cr_2O_3 content increases and the latter proves to be an inert diluent. Completely different is the situation with dimethyl ether and hydrocarbons formation. While the dehydration of the methanol to DME passes through minimum at about 30 wt.% Cr_2O_3, the formation of hydrocarbons reaches a maximum at the same catalyst composition. Summarizing the result presented in Tables 3 and 4 and Figs. 4 and 5 we can conclude that the active component of the mixed catalysts consists of both copper and chromium species. Obviously the association of CuO with Cr_2O_3 leads to a higher methanol conversion to hydrocarbons and lower conversion to dimethyl ether than the sum of conversions on both oxides, i.e., it can be concluded that the synergistic effect occurs over the Cu-Cr/alumina catalysts for methanol dehydration. The same phenomenon was observed by Chang at al. (9) during the investigation of Co oxidation on supported copper-chromium catalysts.

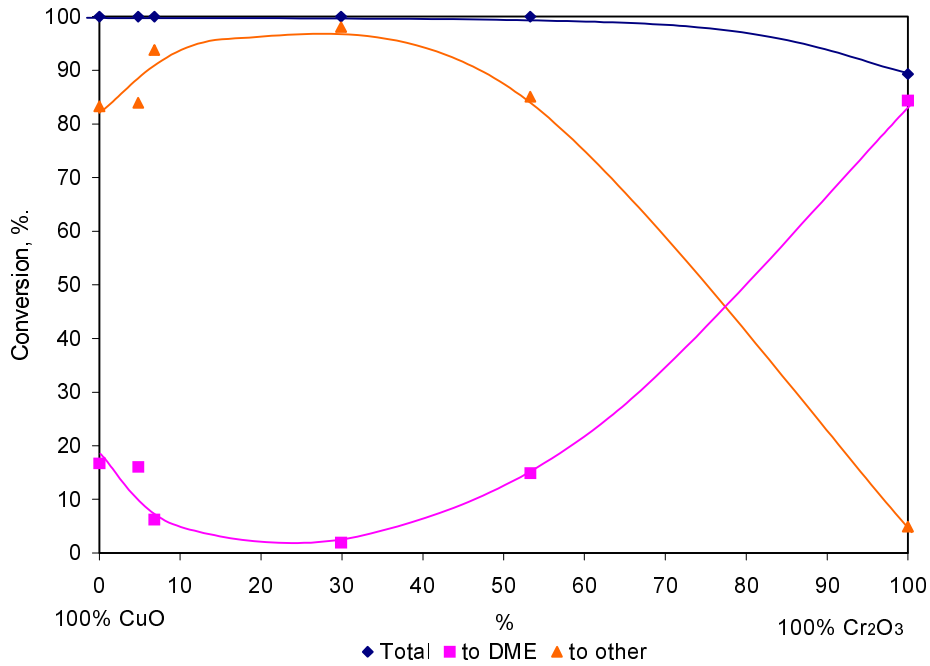

Figure 5. *Product distribution versus catalyst composition at 300°C . Feed gas composition: methanol 4,0 %, nitrogen to 100 %.*

Table 4. *Product distribution versus catalyst composition at 300°C . Feed gas composition: methanol 4,0 %, nitrogen to 100 %.*

Catalyst composition		**Conversion, %**		
Cr_2O_3, %	**CuO, %**	**Total**	**To DME**	**To other products**
0,0	100	100,0	16,7	83,3
4,8	95,2	100,0	16,1	83,9
6,8	93,2	100,0	6,2	93,8
29,9	70,1	100,0	1,9	98,1
53,3	46,7	100,0	14,9	85,1
100,0	0,0	89,3	84,4	4,9

CONCLUSIONS

The catalytic activity of γ–alumina supported CuO – Cr_2O_3 catalysts was researched with regard to methanol dehydration. It was found that these catalysts have enhanced activity toward methanol dehydration. The activity toward dehydration to dimethyl ether strongly depends on the catalyst's composition as follows:

- Alumina supported CuO is a very active catalyst with regard to methanol dehydration, but the selectivity toward DME synthesis is not sufficient. It passes through maximum at 200 – 220°C and rapidly decreases along with the temperature at the expense of increasing the formation of other hydrocarbons.
- Alumina supported Cr_2O_3 is less active, but the selectivity toward DME synthesis is remarkable. The most important feature is that the temperature influence on the selectivity toward DME formation is negligible.

- The mixed CuO – Cr_2O_3 catalysts are very active with regard to methanol dehydration. Full degradation of methanol can be reached even at temperatures lower than 240°C. The increase of Cr_2O_3 leads to a slight decrease of activity. Minimum in selectivity toward DME synthesis and maximum in selectivity toward other hydrocarbons are clearly expressed at 30 wt.% Cr_2O_3 content. A synergetic effect of both copper and chromium species is clearly observed.

REFERENCES

1. Shikada, T.; Fuimoto, K.; Miyauchi, M.; Todriaga, H. Appl. Catal. 1983, 7, 361.
2. Kaeding, W. W.; Butter, S. A. J. Catal. 1980, 61, 155.
3. Chang, C. D. Cat. Rev. Sci. Eng. 1983, 25, l.
4. Bohaeun, L. J. M. Aerosol Rep. 1979, 18, 413.
5. Xu, M.; Lunsford, J. H.; Goodman, D. W. Appl. Catal. A: Gen. 1997, 149, 289.
6. Xu, M.; Goodman, D. W. Appl. Catal. A 1997, 149, 303.
7. Jun, K.-W.; Lee, H. S.; Roh, H. -S.; Park, S. -E. Bull. Korean Chem. Sos. 1998, 19, 446.
8. Jun, K.-W.; Roh, H. -S.; Jae-Woo, K.; Keun, O. J.; Hwan, B. J.; WO20050281004, 2005.
9. Chien, Chin-Cheng; Chuang, Wen-Po; Huang, Ta-Jen; Applied Catalysis A: General 1995, 131, 73.

ПЛОВДИВСКИ УНИВЕРСИТЕТ „ПАИСИЙ ХИЛЕНДАРСКИ“ – БЪЛГАРИЯ
НАУЧНИ ТРУДОВЕ, ТОМ 35, КН. 5, 2007 – ХИМИЯ
UNIVERSITY OF PLOVDIV „PAISII HILENDARSKI“ – BULGARIA
SCIENTIFIC PAPERS, VOL. 35, BOOK 5, 2007 – CHEMISTRY

PREPARATION, CHARACTERIZATION AND CATALYTIC ACTIVITY OF ALUMINA-SUPPORTED COBALT OXIDE FOR DESTRUCTIVE OXIDATION OF ORGANIC COMPOUNDS IN GASEOUS PHASE

M. Stoyanova[1], St. Christoskova[1], P. Konova [2], A. Naydenov[2], M. Georgieva[1]
[1]Department of Physical Chemistry, University of Plovdiv
[2]Institute of General and Inorganic Chemistry, BAS, Sofia

ABSTRACT

Complete oxidation of different volatile organic compounds (VOCs) and CO into harmless water and carbon dioxide using ozone and air as oxidizing agents was investigated over alumina-supported cobalt oxide catalyst. The synthesized catalyst has been characterized by a variety of methods including chemical analysis, IR spectroscopy, X-ray photoelectron spectroscopy, magnetic measurements. The results obtained reveal that the synthesized catalytic system is suitable for catalytic neutralization of exhaust gases from toxic compounds. A significant increase of the catalytic activity and decrease of the reaction temperature was observed using ozone as an oxidant.

Keywords: cobalt oxide, ozone decomposition, CO oxidation, VOCs complete oxidation.

INTRODUCTION

Volatile organic compounds (VOCs) represent a large class of substances emitted from chemical, petrochemical, and allied industries that contribute to both indoor and outdoor air pollution. The damaging effects of VOCs are numerous, ranging from minor annoyances such as eyes, nose, and throat irritation, headaches, and nausea to serious dangers such as damage to the kidneys, liver, and central nervous system. The treatment of such hazardous waste gases in an environmentally acceptable manner and at a reasonable cost is a topic of great universal importance.

An effective, economic and environmentally friendly method for abatement of VOCs is based on heterogeneous catalytic reactions providing complete oxidation. Compared to thermal oxidation, catalytic oxidation can be done at much lower

temperatures. Both noble metal catalysts and metal oxides have been studied extensively for the destruction of VOCs [1-6]. The development of more active metal oxide catalytic systems and using suitable oxidants would be advantageous to provide a low-cost alternative to noble metals for oxidative destruction of VOCs at mild conditions. Cobalt oxides, both unsupported and supported on different oxide support materials (including alumina), have proven their high catalytic activity in the field of air pollution control of CO [7,8] and organic pollutants from effluent streams [9, 10]. In previous papers [11,12] we have described the preparation of a bulk unsupported cobalt oxide system using the oxidation-precipitation method. It has been found that the obtained system has a high catalytic activity in some oxidation reactions, carried out in an aqueous and in a gaseous phase [13,14]. According to the results obtained, the synthesized cobalt oxide system is prominent and useful in a wide field of applications in environmental protection. From a practical point of view it is important to investigate the catalytic properties of this oxide system upon deposition on support materials.

The present study aims to synthesize and characterize an alumina-supported cobalt oxide system (denoted as CoO_x/Al_2O_3), designed as catalyst for low-temperature complete oxidation and to investigate its catalytic activity and selectivity for oxidation of CO and volatile organic substances, using two different oxidants (ozone and oxygen).

EXPERIMENTAL

The CoO_x/Al_2O_3 catalyst was prepared by deposition oxidation-precipitation method in an aqueous solution. A required amount of $Co(NO_3)_2 .6H_2O$ was dissolved in 150 ml of deionised water. An aqueous solution of $Co(NO_3)_2$ was heated up to 70^oC and then, the support - γ-Al_2O_3 was added and kept under continuous stirring for 4 hours. The impregnated catalyst precursor was separated from the solution and subsequently added to a mixture of aqueous solutions of NaOH (4M) and NaOCl (1M). The solid was kept digesting for 24 hours, washed several times (until disappearance of the chlorides), and then dried in an oven at 110^oC for 12 h.

The catalytic activity of the samples was investigated in an isothermal plug flow reactor. The rate of the gas flow was 4.4 l/h, the catalyst volume - 0.2 cm^3, and the mass of the catalyst under consideration - 0.15 g. The inlet concentration of ozone for the reaction of ozone decomposition varied between 22.0 to 24.0 g/m^3. The ozone concentration was analyzed with an Ozomat GM (Germany) ozone analyzer with an accuracy of ± 0.1 g/m^3. The catalytic oxidation of CO and VOCs were carried out within the range of 25 to 110ºC and 25 to 250ºC, respectively. The amounts of CO and VOCs were dosed by an Ismatex MS2/6 (Switzerland) pump. The oxidizing agent being oxygen from synthetic air (gas mixture of 80% nitrogen and 20% oxygen) or ozone produced in oxygen. The inlet concentration of carbon monoxide was 0.18 vol.% and that of VOCs - 0.09 vol.% . The rate of complete oxidation was evaluated by measuring the amount of CO_2 formed during the reaction with a Maihak (NDIR) gas analyzer. The CO and CO_2 concentrations were determined with an accuracy of ± 2 ppm.

RESULTS AND DISCUSSION

The results of chemical analysis and textural characterization of the supported catalyst are listed in Table 1.

Table 1. *The results of chemical analysis, magnetic measurement and textural characterization of the supported CoO_x/Al_2O_3 catalyst*

Co loading in the catalyst [% w/w]	5.16
Co surface density of the catalyst [atoms/nm^2]	2.55
O*/Co atomic ratio of the catalyst	1.51
BET surface area of the catalyst [m^2/g]	207
Total pore volume of the catalyst [cm^3/g]	0.36
Pore size (mean diameter) [nm]	4.8
Magnetic susceptibility of the catalyst χ (.10^6)	-0.12

The supported CoO_x/Al_2O_3 catalyst has a larger surface area than the unsupported one and can be expected to show a higher activity. On the other hand the CoO_x deposition induces a slight decrease of the BET surface area of the initial support, indicating partially blocking of the pores with a smaller diameter of the alumina. The applied synthesis yields mesoporous CoO_x/Al_2O_3 catalyst with mean pore diameter of 4.8 nm.

The IR spectra of the γ-Al_2O_3 support (a), the bulk phase CoO_x (b), the freshly prepared CoO_x/Al_2O_3 catalyst (c) and the used catalyst after ozone decomposition (d) are presented in Fig 1.

As seen from Fig. 1 the spectra of (c) and (d) do not differ essentially, showing that the catalyst structure is not altered during the catalytic reaction. A broad band centered at 3410 cm^{-1} can be attributed to the lattice modes of hydrogen bonded hydroxyl groups, whereas the band at 1640 cm^{-1} corresponds to adsorbed molecular water thus indicating that all the samples are hydrated/hydroxylated.

An intense absorption band at 580 cm^{-1} are observed in both spectra of the (c) and (d) samples. In accordance with the literature data [15], it is assigned to the stretching vibration of the surface cobalt-oxygen bond and also accounts for the presence of active oxygen in the samples. The indicated band is similar to the OB_3 vibrations in the spinel lattice of Co_3O_4 (where B denotes the Co (III) ions in an octahedral coordination), suggesting that the cobalt in CoO_x/Al_2O_3 is situated in an octahedral oxygen environment.

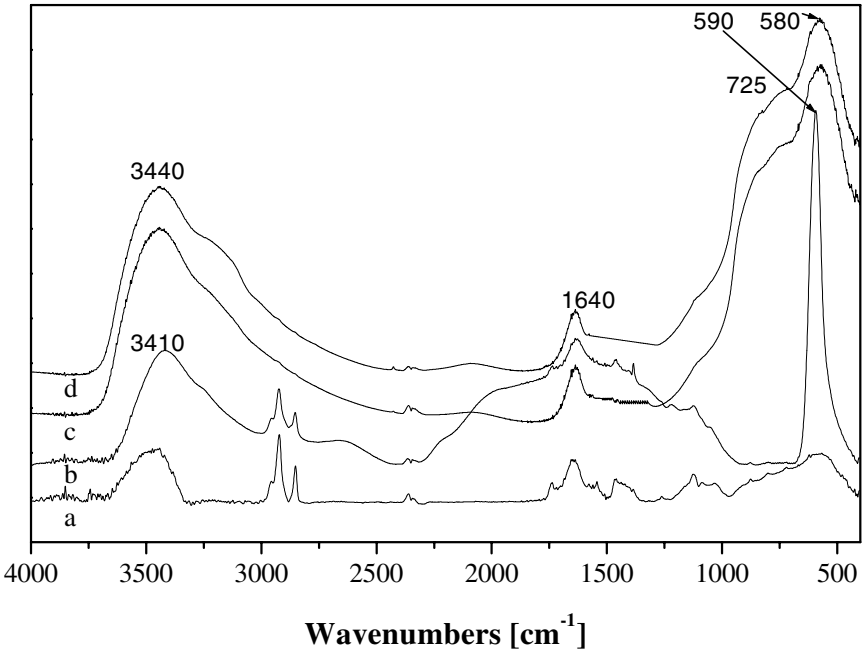

Figure 1. *Infrared spectra of γ-Al_2O_3 support (a), bulk phase CoO_x (b), freshly prepared CoO_x/Al_2O_3 catalyst (c) and used catalyst after ozone decomposition (d).*

The Co2p XPS spectra of fresh and ozonated CoO_x/Al_2O_3 catalysts are shown in Fig. 2 curves *a* and *b*, respectively. The spectra of both samples show similar features, indicating that upon catalytic reaction there is no change in the electronic density of the cobalt atoms. The XPS spectra contain the spin-orbital components $Co2p_{3/2}$ at 780.3 eV and $Co2p_{1/2}$ at 795.3 eV. The measured binding energy values, spin orbit splitting of 15.0 eV and ambiguous satellites imply that the studied samples contain cobalt in a Co^{3+} oxidation state only, present as Co_2O_3. This assumption is confirmed by the magnetic measurement results (Table 1), according to which the CoO_x/Al_2O_3 contains Co(III) (octahedral) ions having t^6_{2g} configuration and being diamagnetic ($\chi = -0.12.10^{-6}$).

Fig. 3 presents the time – conversion dependence of the CoO_x/Al_2O_3 catalyst in ozone decomposition measured at 700 min at three different temperatures: 25ºC, 0ºC and -45ºC. The activity of the catalyst towards ozone decomposition is very high even at temperatures below -40°C and reaches almost 100% at room temperature. Moreover, at each temperature in the beginning the activity is lower and with time followed by increase and stabilization. This behaviour reveals that active species are formed on the surface of the CoO_x/Al_2O_3 catalyst during the catalytic ozone decomposition, which leads to enhancement of the initial activity.

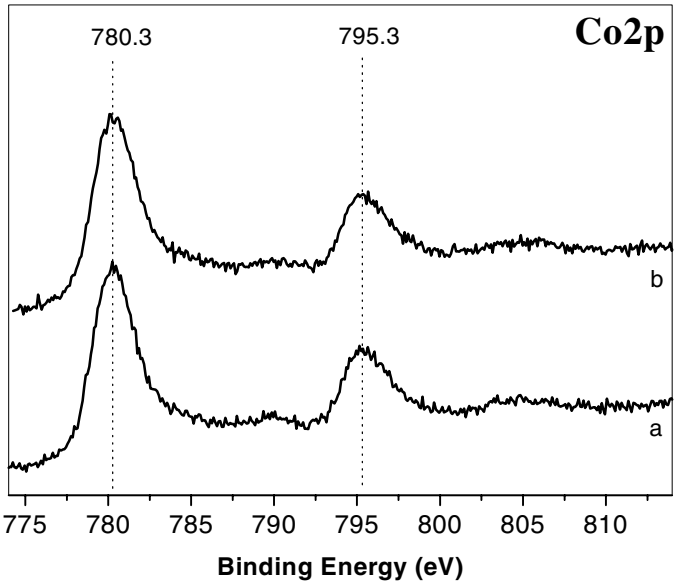

Figure 2. *XPS spectra of fresh (a) and used (b) in reaction of ozone decomposition samples of the CoO_x/Al_2O_3 catalyst*

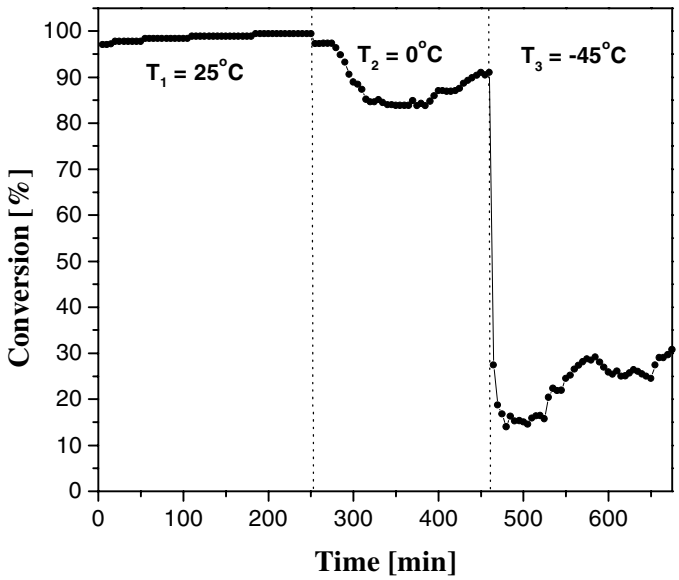

Figure 3. *Conversion – time dependence of the CoO_x/Al_2O_3 catalyst in ozone decomposition at different temperatures*

A significant increase of the catalytic activity of CoO_x/Al_2O_3 catalyst in complete oxidation of different VOCs and CO was observed using ozone as an oxidant instead of air (Figs. 4,5). In fact, the light-off temperature of iso-propanole conversion in presence of ozone is lower with 185°C compared with the case of oxidation in air. Using ozone as oxidant allows carrying out the reaction in low-temperature region (below 80°C) which is extremely substantial in catalytic oxidation of toxic VOCs, because permits saving of energy.

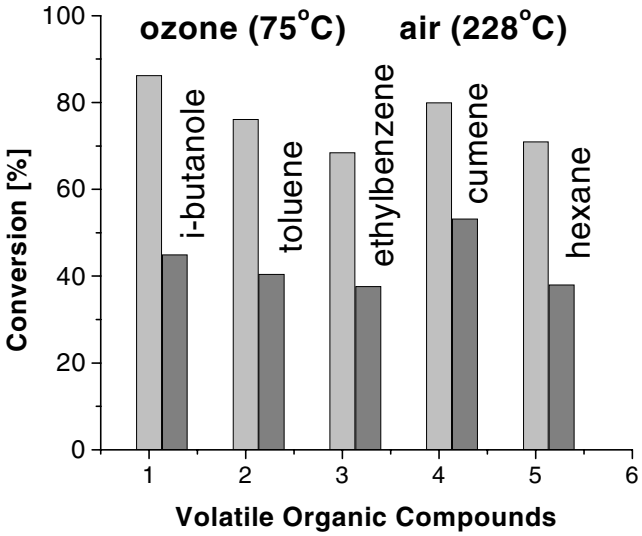

Figure 4. *Comparative study on the catalytic oxidation of different VOCs with ozone and air over CoO_x/Al_2O_3 catalyst*

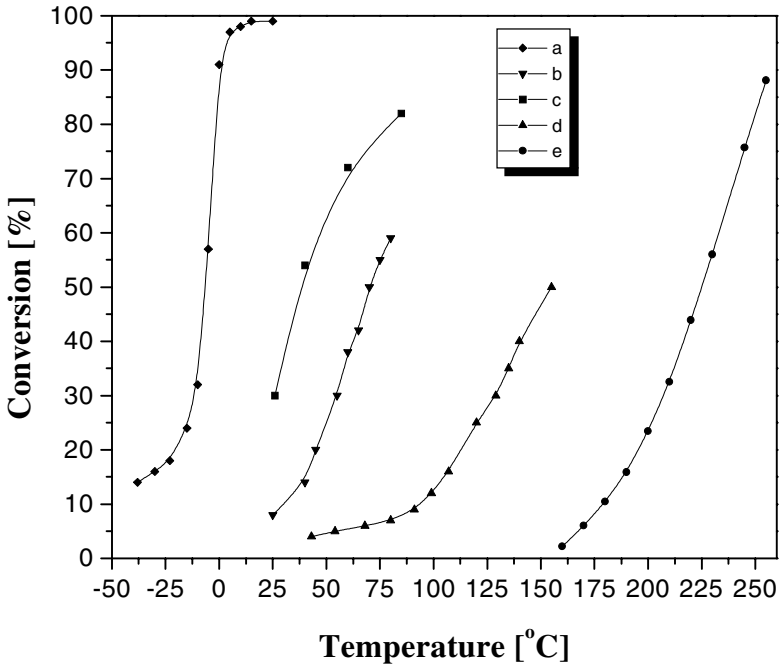

Figure 5. *Conversion - temperature dependences for: (a) - ozone decomposition, (b) - CO oxidation with O_3, (c) - i-propanol complete oxidation with O_3, (d) - CO oxidation with O_2 and (e) - i-propanol complete oxidation with O_2 over CoO_x/Al_2O_3 catalyst*

Two main reasons for the high catalytic activity are found: (i) high content of active and mobile oxygen obtained during the synthesis on the catalyst's surface; (ii) catalytic active complex of O-[Co^{4+}], which is formed during the reaction of ozone decomposition and it is able to oxidize VOCs at room temperatures.

Very important feature of the CoO_x/Al_2O_3 catalyst is that it possesses both activity toward ozone decomposition and ozone oxidation which lead to removing the residual ozone from waste gases. Hence the CoO_x/Al_2O_3 catalyst is very suitable for application in environmental catalysis.

ACKNOWLEDGEMENTS

Authors gratefully acknowledge the financial support by the National Science Fund at the Ministry of Education and Science of Bulgaria (Project VUX-1105) and from the University of Plovdiv Research Fund (Project 07-X-70).

REFERENCES

1. Q. Dai, X. Wang, G. Lu, Catal. Commin. 8 (11) (2007) 1645.
2. F. Bertinchamps, M. Treinen, P. Eloy, et al., Appl. Catal. B : Environ. 70 (1-4) (2007) 360.
3. M. C. Alvarez-Galvan, B. Pawelec, J.L.G. Fierro, et al., Appl. Catal. B : Environ. 51 (2) (2004) 83.
4. T. Ataloglou, C. Fountzoula , K. Bourikas et al., Appl. Catal. A 288 (1-2) (2005) 1.
5. L.-M. Shi, W. Chu, M.-H. Chen, J.-Q. Xu, Modern Chem. Ind. 26 (5) (2006) 24.
6. R. Lopez-Fonseca , J. Gutierrez-Ortiz , J. Gonzalez-Velasco , React. Kinet. Catal. Lett. 86 (1) (2005) 127.
7. Y. I. Mergler, J. Hoebink, B. E. Nieuwenhuy, J. Catal. 167 (1997) 305.
8. J. Jansson, J. Catal. 194 (2000) 55.
9. E. Garbowski, M. Guenin, M. C. Marion, M. Primet, Appl. Catal. B 64 (1990) 209.
10. A. K. Sinha, V. Shankar, J. Chem. Eng. Biochem. Eng. 52 (1993) 115.
11. St. Christoskova, M. Stojanova, M. Georgieva, D. Mehandjiev, Mater. Chem. and Phys. 60 (1999) 39.
12. St. Christoskova, M. Stojanova, M. Georgieva, D. Mehandjiev, Thermochim. Acta, 292 (1997) 77.
13. St. Christoskova, M. Stojanova, M. Georgieva, O. Argirov, React. Kinet. Catal. Lett. 66 (1) (1999) 55.
14. St. G. Christoskova, M. Stoyanova, G. Ivanov, D. Mehandjiev, Bulg. Chem. Comm. 30 (1-4) (1998) 470.
15. A. Bielanski and J. Haber, Oxygen in Catalysis, Marcel Dekker Inc., New York, 1991.

ПЛОВДИВСКИ УНИВЕРСИТЕТ „ПАИСИЙ ХИЛЕНДАРСКИ“ – БЪЛГАРИЯ
НАУЧНИ ТРУДОВЕ, ТОМ 35, КН. 5, 2007 – ХИМИЯ
UNIVERSITY OF PLOVDIV „PAISII HILENDARSKI“ – BULGARIA
SCIENTIFIC PAPERS, VOL. 35, BOOK 5, 2007 – CHEMISTRY

BIOSENSOR FOR XANTHINE WITH IMPROVED SENSITIVITY AND DETECTION LIMIT

T. Dodevska[1], E. Horozova[2], N. Dimcheva[2]
[1] Dept Inorganic & Physical Chemistry; University of Food Technology;
26, Maritza blvd., 4002 – Plovdiv
[2] Dept Physical Chemistry, University of Plovdiv;
24, Tsar Assen st., 4000 – Plovdiv
E – mails: dodevska@mail.bg; horozova@uni-plovdiv.bg

ABSTRACT

An interference-free amperometric biosensor for the quantitative xanthine analysis is described. Xanthine was monitored through the electrochemical reduction of hydrogen peroxide (produced upon its enzyme-catalyzed oxidation) at a constant applied potential of -50 mV (vs. Ag/AgCl). The biosensor was designed on the basis of a graphite electrode modified with microquantities of platinum and palladium (mixed in the ratio 30% Pt : 70% Pd). The analytical performance of the produced biosensor was compared with previously reported results obtained with a different basic transducer (graphite modified with 10% Pt : 90% Pd). The here presented biosensor exhibits operational characteristics, such as electrode sensitivity, linearity range and detection limit much better than the earlier reported.

Keywords: Modified graphite electrodes, Hydrogen peroxide electroreduction, Xanthine oxidase, Xanthine, Biosensor.

INTRODUCTION

Determination of xanthine (uremic toxin) in human blood and urine is important in clinical assays – it is one of the most widely used markers to assess renal function.

The levels of xanthine in plasma and urine samples are routinely measured by such analytical techniques as high-performance liquid chromatography (HPLC) [1,2,3], chemiluminescence (CL) [4], or UV-spectroscopy, whose common drawback is the painstaking procedures for sample preparation. In contrast, an electrochemical biosensor, which combines the high substrate specificity of a chosen biological catalyst (e.g. an enzyme) with the simplicity of operation with electrochemical

equipment, would offer the advantages of a rapid, highly selective, compact, and convenient for handling method for the determination of the target analyte. In addition, it is cost-effective since a small amount of the immobilized enzyme can be repeatedly used for up to several hundreds of assays.

The detection of xanthine with amperometric biosensors, reported so far in the literature is achieved through:

i) electrochemical oxidation of the reaction products such as uric acid and hydrogen peroxide (both produced upon enzymatic oxidation of the analyte) [5, 6];

ii) the redox conversion of organic compounds capable of effectively shuttling electrons between the enzyme active site and the electrode (so-called mediators) [7-11]. As efficient mediators for xanthine oxidase electrochemical transformation as low-molecular weight species, freely diffusing between the electrode surface and the enzyme, such as cobalt phtalocyanine [7] and Prussian blue [8], as organic polymers in which the enzyme was incorporated [9-11]. The later afford the opportunity for developing reagentless enzyme electrodes, since the mediator is assembled together with the biocatalyst on the transducer surface. The applicability of all these biosensors to detecting xanthine in blood serum and urine samples was proven.

A substantial problem in biosensors design is to find the way to eliminate the unwanted electrochemical transformation of interfering substances, present in real samples. The use of a Nafion membrane or other polyelectrolyte multilayer films [12] to block the access of electroactive species to the electrode surface has been reported.

Our research is focused on the development of a simple, sensitive enzyme electrode with interference-free response, which can be used for quantitative determination of xanthine in mammalian bio-liquids. In this paper an amperometric xanthine biosensor with improved sensitivity and detection limit is described. A modified graphite matrix, effective in the elimination of the interferences from uric acid, ascorbic acid and glutathione is used as the basic electrode.

EXPERIMENTAL

Materials

Xanthine oxidase (XOD) (E.C. 1.1.3.2) from buttermilk (Fluka) with an homogeneous activity 8 U mg^{-1} (1 U corresponds to the amount of enzyme which oxidizes 1 μM xanthine per minute at pH 7.5 and 25^0C); xanthine , H_2O_2, uric acid, L-ascorbic acid, glutathione and the chemicals used to prepare buffer solutions: $Na_2HPO_4.12H_2O$, KOH and H_3PO_4, were purchased from Fluka. Gelatine – analytical grade (Chimtek, Bulgaria) was employed as a 5% suspension in phosphate buffer (pH=8.4) for electrode coating formation. All solutions were prepared with bidistilled water.

Preparation of the electrode

Inert pads of graphite (type GMZ with geometric surface area S=1.6 – 1.8 cm^2; 0.7x0.7x0.3 cm) were used. The structural characteristics of this graphite are as

follous: specific surface 0.8 $cm^2 g^{-1}$, density 1.56 – 1.7 g cm^3, porosity 20 – 25%. The graphite pads were modified with microqantities of platinum and palladium mixed in the ratio Pt:Pd 30%:70%. The catalytically active components were deposited in a potentiostatic regime ($Er^{deposit}$= + 0.05V vs. reversible hydrogen electrode) via a brief electrolysis ($t_{deposit}$=10 s) from the following electrolyte: 2%$PtCl_6.6H_2O$ + 2% $PdCl_2$ + 0.1M HCl in the ratio Pt:Pd (30:70%) [6].

Enzyme immobilization

The enzyme immobilization was carried out on an electrochemically activated electrode surface. The electrochemical pretreatment of the modified graphite electrode started with a cathode-anode cycling (30 min) within the potential range from -0.60 to +0.35 V (vs. Ag|AgCl). Just before immobilization, the electrode was polarized for 2 min at E = 1.5 V. The adsorption of XOD was carried out under static conditions by immersing the graphite electrode in the enzyme solution with a 10^{-5} M concentration, in phosphate buffer (pH = 8.4) for 24 h at 4^0C. After adsorption the electrode was dried in the air, at room temperature, for about 45 min. Then the working surface of the prepared electrode was coated with a layer of 5% gelatine solution containing XOD (5 mg XOD in 1 ml 5%-gelatine solution at 37 °C) using a capillary glass tube. After applying the layer, the electrode surface was dried with argon.

After completing the measurements the enzyme electrode was carefully washed with bidistilled water, dried in the air at room temperature for about 30 min and then stored in a refrigerator at 4 °C until measurement. When necessary, the immobilized enzyme could be removed from the electrode surface by treating of the electrode for ~20 min in hot doubly distilled water (50 – 60 °C) thus regenerating the bare modified graphite electrode. The processed electrode material can be stored for more than one year in bi-distilled water (at room temperature) and used repeatedly.

The analytical performance of the enzyme electrodes based on Pt:Pd(30:70)/Cgmz and Pt:Pd (10:90)/Cgmz (which will be further denoted in the text as EE type B and EE type A, respectively), were compared. The later was fabricated according to a previously reported protocol [6].

Apparatus and measurements

All electrochemical measurements were performed in a three-electrode cell with separated compartments (working volume 11-15 mL). An Ag|AgCl electrode was used as a reference electrode, and platinum wire as a counter electrode. The electrochemical setup also involved a bipotentiostat, type BiPAD (TACUSSEL, Villeurbanne, France); a generator, type EG-20 (Elpan, Lubawa, Poland); a digital voltmeter, type 1AB105 (ZPU, Pravets, Bulgaria). The solutions were bubbled with argon during the measurements.

The amperometric data were obtained by successive addition of aliquots of $8.6.10^{-4}$ M xanthine solution to the phosphate buffer in the cell with simultaneous registration of the current at constant potential. The time to reach a steady-state value of the current did not exceed 2 min.

For maintaining constant temperature a thermostat UH (VEB MLW Prüfgeräte - Werk, Medingen, Germany) was used. The pH of the buffer solutions was adjusted with a pH-meter OP - 208 (Radelkis, Budapest, Hungary).

RESULTS AND DISCUSSION

A series of modified graphites, based on the commercially available graphite (type GMZ) whose surface was modified with micro- and nano-deposits of catalytically active components (consisting of Pt and Pd mixed in various ratios) was tested as electrode materials at the electrochemical reduction of hydrogen peroxide. The graphite modified with 30% Pt : 70% Pd was chosen as the basic transducer for designing the xanthine biosensor since it showed an excellent electrochemical performance at the process of interest (electroreduction of H_2O_2). This electrode showed both the lowest background current and the highest sensitivity (dI/dC=0,82 ± 0,02 $\mu A.\mu M^{-1}$) in combination with wide range strict linear dependence of the electrode response (up to 600 μM) at an applied potential of –50 mV (Ag/AgCl) [13].

High selectivity of the assay is one of the factors of crucial importance to consider when developing amperometric biosensors, because a waste variety of electrochemically active species are normally present in the real samples, which can potentially contribute to the output response thus compromising the analytical results. In this connection, it should be pointed out that the modified graphite demonstrated full inertness towards a variety of potentially interfering compounds. Under the selected experimental conditions no electrochemical response was achieved to uric acid, ascorbic acid or glutathione, present in the concentration of 10^{-5} M, which exceeds the possible physiological levels.

The polarization curves of modified electrode over the potential range from -300 to +300 mV (Ag/AgCl) in the presence of 10^{-4} M H_2O_2 were examined at both pH=7 and pH=8.4, as depicted at Fig.1. The potential ranges where the reduction current reaches limited values (plateau region) were found nearly the same at both pH investigated. A slightly extended plateau region (from –150 mV to +150 mV) was observed at pH 8.4 as compared to pH 7.0, where the plateau lies between –150 mV and +50 mV.

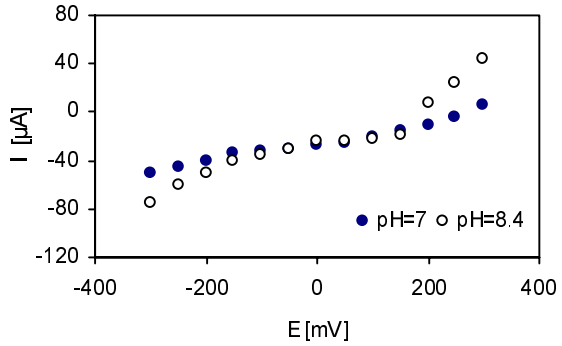

Figure 1. *Polarization curves of graphite modified electrode Pt:Pd(30:70)/Cgmz in 0.1mM H_2O_2, background electrolyte: phosphate buffer; reference electrode Ag/AgCl; temperature 20^0C*

Modified graphite electrode Pt:Pd(30:70)/Cgmz was used as the basic transducer for developing an amperometric xanthine biosensor for highly selective quantitative analysis of xanthine through immobilization of XOD according to an already reported protocol [13] (EE type B).

Operational parameters determined for the EE type B at an applied potential of -50 mV (vs. Ag/AgCl) at 25^0C are presented in Table 1. The linearity range for this enzyme electrode was found twice as large as for the EE type A, while the sensitivity of the first one was estimated to be almost one order of magnitude higher than the sensitivity of the later. The calibration graph (Fig.2-A) shows strict linear dependence of the steady-state electrode response (for the EE type B) on xanthine concentrations up to 70 μM; the electrode sensitivity was determined as the slope of the linear portion of the calibration graph as 0.39 $\mu A.\mu M^{-1}$. At substrate concentrations exceeding 80 μM XOD, the calibration graph turnes to a horizontal line, which most probably is due to the enzyme saturation with xanthine. The biosensor produced demonstrated considerably lower detection limit to xanthine – 1.5 μM (determined at signal to noise ratio 3:1) as compared to 4.5 μM for EE type A. The better analytical performance of the EE type B as compared to the EE type A could be ascribed to several factors acting synergistically. From the one hand, the basic transducer for designing the EE type B possesses enhanced catalytic activity and sensitivity towards hydrogen peroxide electrochemical reduction. From the other, the immobilized on its surface xanthine oxidase was chosen with higher homogeneous activity than this ane used to develop the EE type A.

The apparent Michaelis constant Km^{app} , which is a basic kinetic parameter, was calculated both from the Lineweaver-Burke plot (1/C vs 1/I) (Fig 2-B) and Eadie-Hofstee plot (not shown). The obtained values were found practically identical: Km^{app}=58.4 μM (r^2=0.996) determined from the LB-plot; and Km^{app}=58.6 μM (r^2=0.995) estimated using the EH-method. Higher Km^{app} value than this reported for EE type A results in wider linearity range for the xanthine biosensor type B.

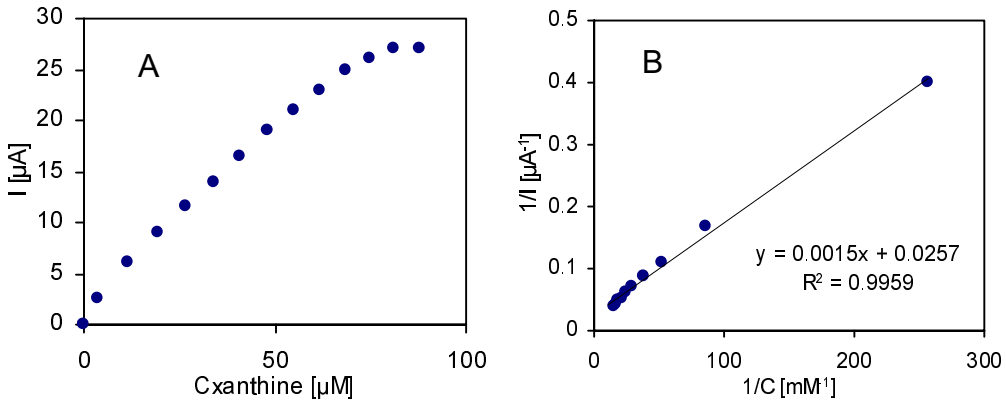

Figure 2. *A - Steady-state response of the enzyme electrode type B as a function of xanthine concentration; B – Lineweaver – Burke plot. Applied potential -50mV(vs. Ag/AgCl); background electrolyte: 0.1 M phosphate buffer, pH=8.4; temperature 25 ^{0}C*

CONCLUSIONS

The enzyme electrode with considerably improved operational characteristics was prepared using graphite electrode modified with Pt and Pd, mixed in the ratio 30%:70% and XOD with higher homogeneous activity, than previously used [6]. The enzyme electrode produced, tested under the selected experimental conditions (ambient temperature, 25^0C; working potential -50mV; pH 8.4) showed the following operational characteristics:

- a detection limit of 1.5 μM;
- a linear range up to 70 μM;
- a sensitivity of 0.39 $\mu A.\mu M^{-1}$;
- no response to glutathione, ascorbic acid and uric acid present in higher than the physiological levels.

A brief comparison of the xanthine biosensor presented here with previously published results [6] (accomplished with an enzyme electrode based on graphite modified with 10%Pt+90%Pd) showed that the new biosensor displayed better electrode sensitivity with larger linear range, lower detection limit and higher selectivity (practically inert towards interference substances as ascorbic acid, uric acid and glutathione).

Table 1. *Operational parameters of xanthine oxidase-based enzyme electrodes; working potential -50mV (vs. Ag/AgCl); background electrolyte phosphate buffer pH=8.4; temperature 25^0C*

Enzyme electrode type	Sensitivity, $\mu A.\ \mu M^{-1}$	r^2	Linearity, μM	Detection limit, μM	I_{max}, μA	Km^{app}, μM
EE type A	0.3	0.98_4	40	4.5	10	30
EE type B	0.39	0.98_3	70	1.5	39	58.5

AKNOWLEDGMENT

Financial support from the University of Plovdiv Research Fund is gratefully acknowledged.

REFERENCES

1. H. Shahbazian, H. Mombini, A. Moghaddam, M. Jasemi, Urology Journal, 3, 225-229, (2006)
2. S. Sugase, T. Tsuda, BUNSEKI KAGAKU Abstracts 51, (2002)
3. V. Samanidou, A. Metaxa, I. Papadoyannis, Journal of liquid chromatography & related technologies, 25, 43-57, (2002)
4. J. Hlavay, S. Haemmerli, G. Guilbault, Biosensors&Bioelectronics, 9, 189-195, (1994)
5. Z. Junguo, J. O `Daly, R. Henkens, J. Stonehuerner, A. Crumbliss, Biosensors& Bioelectronics, 11, 493-502, (1996)

6. N. Dimcheva, E. Horozova, Z. Jordanova, Z. Naturforsch, 57, 883-889, (2002)
7. E. Kilinc, A. Erdem, L. Gokgunnec, T. Dalbasti, M. Karaoglan, M. Ozsoz, Electroanalysis, 4, 273-275, (1998)
8. Y. Liu, L. Nie, W. Tao, S. Yao, Electroanalysis, 16, 1271-1278, (2004)
9. Y. Miao, X. Wu, J. Chen, Chem. Anal. (Warsaw), 50, 507, (2005)
10. H. Xue, S. Mu, Journal of electroanalytical chemistry, 397, 241-247, (1995)
11. M. Rahman, M. Won, Y. Shim, Electroanalysis, 19, 631-637, (2007)
12. T. Hoshi, T. Noguchi, J. Anzai, Materials Science and Engineering, 26, 100-103, (2006)
13. T. Dodevska, E. Horozova, N. Dimcheva, Anal. Bioanal. Chem., 386, 1413-1418, (2006)

ПЛОВДИВСКИ УНИВЕРСИТЕТ „ПАИСИЙ ХИЛЕНДАРСКИ“ – БЪЛГАРИЯ
НАУЧНИ ТРУДОВЕ, ТОМ 35, КН. 5, 2007 – ХИМИЯ
UNIVERSITY OF PLOVDIV „PAISII HILENDARSKI“ – BULGARIA
SCIENTIFIC PAPERS, VOL. 35, BOOK 5, 2007 – CHEMISTRY

KINETICS OF ANODE PROCESSES IN *CHROMISPEL - C* ELECTROLYTE FOR CHROMIUM PLATING

R. Mantcheva, K. Kanchev, N. Milcheva
The University of Plovdiv, Department of Physical Chemistry,
24 Tsar Assen Street, 4000 Plovdiv, BULGARIA

ABSTRACT

The kinetics of anode process running in Chromispel – C non-standard chloride electrolyte for chromium plating has been studied. The anodes investigated are prepared from platinum, silver, lead, PbCa 0.11% alloy and M10 and P25 ceramal alloy. The processes running on the anode are identified. The distribution of the total current among anode reactions is established. The effect of electrolyte concentration, anode material, current density and temperature on current distribution is studied.

The potential dynamic curves are recorded under varying operation conditions of chromium plating and the general I vs. E dependence established. The values of the corresponding corrosion potentials E_c, potentials E_1 and E_2 as well as the limiting currents I_1 and I_2 for the first and second step of the I vs. E curve are determined.

The activation energy is calculated using the temperature-kinetic model and the mechanism of electrode polarization established.

Platinum and P25 ceramal alloy are recommended as suitable anode materials.

Keywords: Chromium plating, anode materials, cermal alloy, electrodeposition.

INTRODUCTION

The majority of plants around the world use the standard chromium bath while chrome plating (containing chromium trioxide 250 $g.L^{-1}$ and 2.5 $g.L^{-1}$ sulfuric acid). In this bath, chromium deposits with current efficiency not higher than 10 – 12%. This low efficiency is one of the reasons to constantly search for new, more effective components and techniques of chrome plating.

“Chromispel” baths can be referred to the new electrolytes. They are characterized with exceptionally high content of chromium trioxide (up to 1600 $g.L^{-1}$) and there the sulfate anions are replaced with halogens (Cl^-, I^-). The perceptiveness of these electrolytes is determined by the fact that they create possibility for electroplating of layers with current efficiency 60 to 70% at room temperature /1-5/.

The practical usage of *Chromispel* electrolytes is made difficult because of the lack of suitable anode materials. They are supposed to possess not only high resistance to corrosion in the aggressive media of the chrome bath, but to guarantee suitable distribution of the total anode current, i.e. a small quantity of chlorine should be precipitated over them and the oxidation of the trivalent chrome ions should run with such a speed, at which they do not accumulate in the chromium bath.

In the NAFTA countries in a report, represented to the Senate of USA it is commented that during 2004 the galvanic production decreased with 75% in comparison to 2000, because of the export of a big part of the automobile production in China. In order to avoid these important economical problems it is recommended to galvanic specialists to search for new materials and new technologies of chrome plating.

EXPERIMENTAL CONDITIONS AND SET-UP

Preparation of Chromispel – C electrolytes

Electrolytes with different content of CrO_3 were prepared:

- electrolyte of *standard* concentration - CrO_3 *250* $g.L^{-1}$
- electrolyte of *middle* concentration - CrO_3 *500* $g.L^{-1}$
- electrolyte of *high* concentration - CrO_3 *750* $g.L^{-1}$.

To each of them it was added a different quantity of hydrochloric acid in CrO_3 : Cl^-; 15:1, 20:1, 25:1, 30:1 ratio.

Experimental conditions for collecting and separating of the anode gas

For the defining of the composition of the anode gasses at deposition of chrome from chloride electrolyte it was used the Orsa apparatus, equipped with burette and absorption vessel only for the chlorine. The volume of oxygen was determined as a different from the total volume of the anode gasses and the volume of the absorbed chlorine by the absorbent agent.

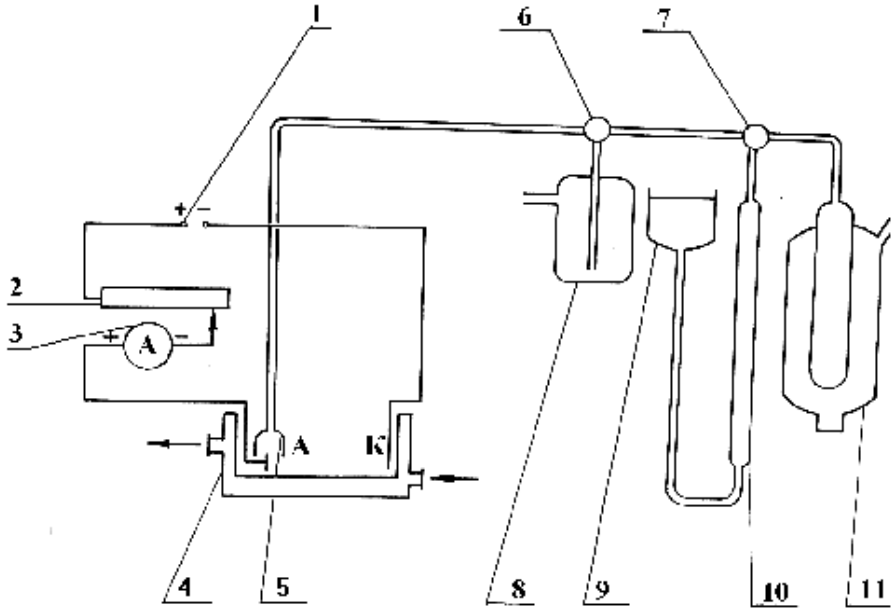

Figure 1. *Scheme of the experimental conditions: 1– rectifier; 2 – rheostat; 3 – ampere meter; 4 – galvanic cell; 5 – collective bell for anode gases; 6, 7 – three-way taps; 8 – hydraulic shutter; 9 – pressure vessel; 10 – measuring burette; 11 – absorber*

Experimental conditions for taking down of the polarization curves

In order to take down the polarization curves we used: RADELKIS potentiostat OH - 405 type, XY – RECORDER and reference Calomel electrode. The cathode was a copper plate, for the anode we used platinum.

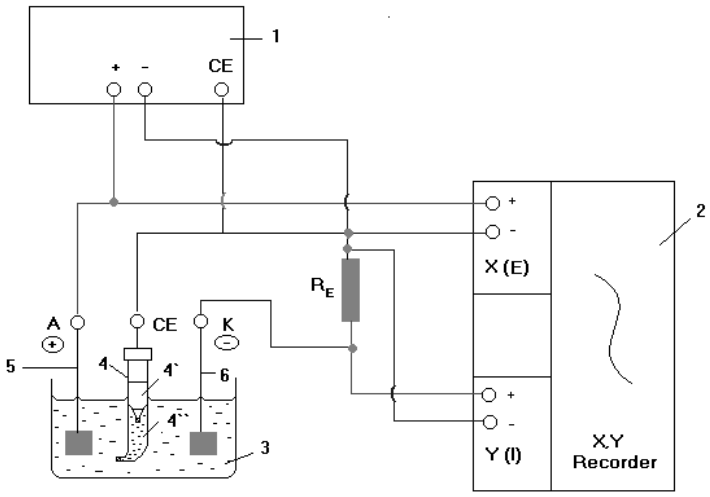

Figure 2. *Scheme of the equipment for recording polarization curves in potentiostatic regime: 1 - potentiostat; 2 – recorder; 3 – electrolysis bath; 4 – reference electrode (Calomel electrode); 4` - salt bridge; 5 - anode; 6 – cathode; R_E – high ohm resistance*

RESULTS AND DISCUSSIONS

Platinum was chosen to be an anode because of its high electrochemical stability in *Chromispel – C* electrolyte. This anode material guarantees the cleanness of the experiment, which means that in the electrolyte there will not be any foreign ions, apart of those included in its composition. While chrome plating with *Chromispel – C* electrolytes a minimum of three partial reactions run – evolution of oxygen, evolution of chlorine and oxidation of trivalent chromium ions to hexavalent ones.

$$1)\ 2Cl^- - 2e^- \rightarrow Cl_2$$

$$2)\ 4OH^- - 4e^- \rightarrow O_2 + 2H_2O$$

$$3)\ Cr^{3+} - 3e^- \rightarrow Cr^{6+}$$

The smallest part of the total anode current is spent on evolution of chlorine and the biggest possible one for the obtaining of oxygen (Figure 3). The chrome plating conditions influence that distribution. The high anode density leads to the increase of A_{Cl_2} and A_{O_2} and to decreasing of that of $A_{Cr^{3+}/Cr^{6+}}$.

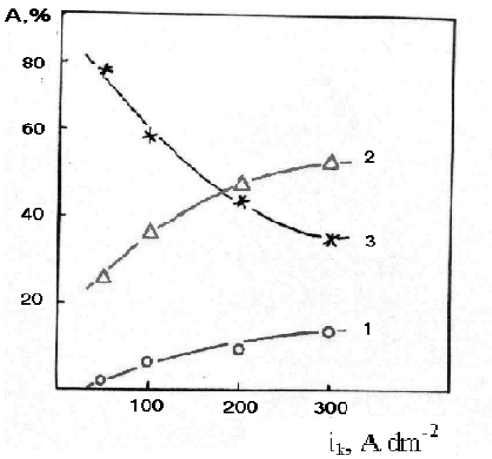

Figure 3. *Current efficiency for the three anode partial reactions on platinum anodes in medium concentration of Chromispel –C electrolyte, calculated in percentage; 1 – curve for separating of chlorine, 2 – for oxygen, 3 – for oxidation of trivalent chrome ions to hexavalent ones*

It was established that the presence of 2 to 6 g trivalent chrome ions influence slightly on the electrochemical evolution of oxygen and oxidation of trivalent chrome ions to hexavalent chrome ions, at the same time lowers abruptly current efficiency A_{Cl_2} (Figure 4).

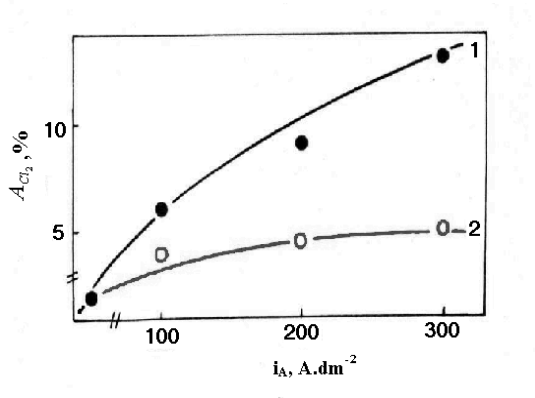

Figure 4. *Influence of the trivalent chrome ions on current efficiency of the reaction* $2Cl^- - 2e^- \rightarrow Cl_2$ *in medium concentration of Chromispel – C electrolyte at 20ºC; 1 – without* Cr^{3+}, *2 – with 6 g.L*$^{-1}$ Cr^{3+}

By taking down potential dynamic curve the polarization dependencies are studied in *Chromispel – C* electrolytes for platinum anodes. The influence of the factors was studied – concentration of chromium trioxide and hydrochloric acid, temperature, influence of trivalent chrome ions and nature of the anode material. The value of the corrosion potential has been estimated (E_c) as function of those factors. It is from 1,19 to 1,29 V and is little influenced by the conditions of electrolysis (Tables 1, 2, 3).

Table 1. *Values of E_c, measured in Chromispel – C electrolyte with a concentration of 250 g.L*$^{-1}$ *and platinum anode, calculated according to Calomel electrode*

t^{0}C	CrO_3:Cl^-	E_c, V	CrO_3:Cl^-	E_c, V	CrO_3:Cl^-	E_c, V	CrO_3:Cl^-	E_c, V
20	15:1	1,2471	20:1	1,2071	30:1	1,2571	35:1	1,2171
30		1,2105		1,1905		1,2105		1,2205
40		1,2040		1,2640		1,2340		1,1740
50		1,1875		1,2375		1,2275		1,2275

Table 2. *Values of E_c, measured in Chromispel – C electrolyte with a concentration of 500 g.L*$^{-1}$ *and platinum anode, calculated according to Calomel electrode*

t^{0}C	CrO_3:Cl^-	E_c, V	CrO_3:Cl^-	E_c, V	CrO_3:Cl^-	E_c, V	CrO_3:Cl^-	E_c, V
20	15:1	1,2571	20:1	1,2671	30:1	1,2471	35:1	1,2271
30		1,2205		1,2105		1,2105		1,2105
40		1,2640		1,2940		1,2040		1,2140
50		1,2475		1,2275		1,2275		1,2275

Table 3. *Values of E_c, measured in Chromispel – C electrolyte with a concentration of 750 g.L*$^{-1}$ *and platinum anode, calculated according to Calomel electrode*

t^{0}C	CrO_3:Cl^-	E_c, V	CrO_3:Cl^-	E_c, V	CrO_3:Cl^-	E_c, V	CrO_3:Cl^-	E_c, V
20	15:1	1,2371	20:1	1,2971	30:1	1,2871	35:1	1,2771
30		1,2705		1,2905		1,2605		1,2605
40		1,3040		1,2940		1,2940		1,2840
50		1,3075		1,2975		1,2975		1,2975

It has also been found the general type of the anode polarization curve for platinum anode (Figure 5). It is characterized with two steps, the first of which is more clearly expressed and the limit current I_1 corresponds to it, while the second corresponds to current I_2. I_1 is changed from $0{,}55*10^{-3}$ A to $5*10^{-3}$ A, but I_2 has values of $3{,}9*10^{-3} – 37*10^{-3}$ A.

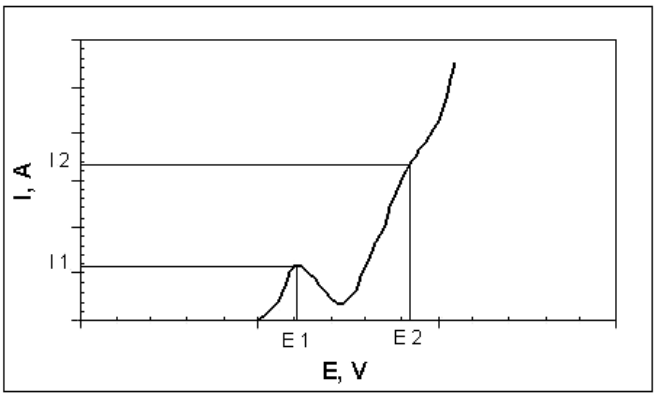

Figure 5. *General type of the anode polarization curve, taken down at 20ºC in Chromispel – C electrolyte*

The potential corresponding to I_1 is very close to the standard potential of the reactions – discharging of oxygen and oxidation of trivalent chrome ions to hexavalent ones. This proximity does not let us clarify which of the two reactions starts first.

$$2H_2O \rightarrow O_{2(г)} + 4H^+ + 4e^-, \qquad E^0 = 1{,}229V$$

$$7H_2O + 2Cr^{3+} \rightarrow Cr_2O_7^{-2} + 14H^+ + 6e^-, \qquad E^0 = 1{,}33V$$

Through experiment it has been proved that the lower the potential of the electrode has been, the higher A_{O_2} has been. With the increasing of the potential and current the quantity of the discharged gas chlorine increases, that's why we can say with certainty that the second step corresponds to the discharging of chlorine.

$$2Cl^- - 2e^- \rightarrow Cl_2$$

Table 4. *Anodic current efficiency for the separate anode reactions in Chromispel – C, 500 g.L^{-1} CrO_3, CrO_3:Cl^-=20:1, t=20^{0}C*

τ , h	I, A	E, V	i, A.dm^{-2}	V_{Cl_2} , ml	V_{O_2} , ml	A_{Cl_2} ,%	A_{O_2} ,%	$A_{Cr^{3+}/Cr^{6+}}$,%
5	0.12	**1.7**	4	8	12	3.19	**9.57**	87.24
2.5	**0.21**	**1.9**	7	**33.8**	1.2	15.4	1.1	83.5

The obtained values of the potentials for the first and second step E_1 and E_2 from the polarization curves are higher than the corresponding standard potentials. This is

to say that the electrochemical processes, running on the anode, are connected with significant polarization.

Through using of temperature – kinetic method it has been calculated E_a and it has been determined the nature of the electrode polarization. The types of polarization are concentration, electrochemical and phase. At concentration polarization E_a of 8380 – 25140 J.mol^{-1} and it does not change with alteration of the potential. For the first step the numerical values correspond to the concentration polarization but with the alteration of the potential E_a is changed which is an evidence of electrochemical hindrance.

Table 5. *Values of Ea calculated from the dependency $lni_1 – 1/T$ in Chromispel – C electrolyte with concentration of 250g.L^{-1} CrO_3*

CrO_3:Cl^-	Values of E trough which isopotential lines pass, V	E_a, J.mol^{-1}
15:1	1,125	4365
	1,25	35334
	1,375	12877
20:1	1,125	3118
	1,275	2494
	1,4	2078
30:1	1,15	7690
	1,25	6651
	1,45	3326
35:1	1,175	8730
	1,35	13302
	1,475	3949

E_a, which corresponds with the reaction of the chlorine evolution, is several times bigger than the one for the evolution of oxygen, but its numerical values are still in the limits, typical for concentration polarization.

Table 6. *Values of E_a calculated from the dependency $lni_2 – 1/T$ in Chromispel –C with concentration of 250 g.L^{-1} CrO_3, CrO_3:Cl^-=20:1*

Values of E trough which isopotential lines pass, V	E_a, J.mol^{-1}	tgα
1,75	17460	2100
1,85	19538	2350
1,925	21201	2550

As the influence of the nature of the anode material is essential for the kinetics of the anode processes, we have paid attention to pure silver anodes, pure lead ones and the alloy PbCa (0,11% Ca) which was especially designed for this research by the Bulgarian Academy of Sciences. Metal ceramal alloys M 10 and P 25 were observed

too (Figure 6). It was also found that the lowest E_c is in the alloy PbCa (0,11%Ca) (-0,32V), and the highest is that of M 10 (0,63V).

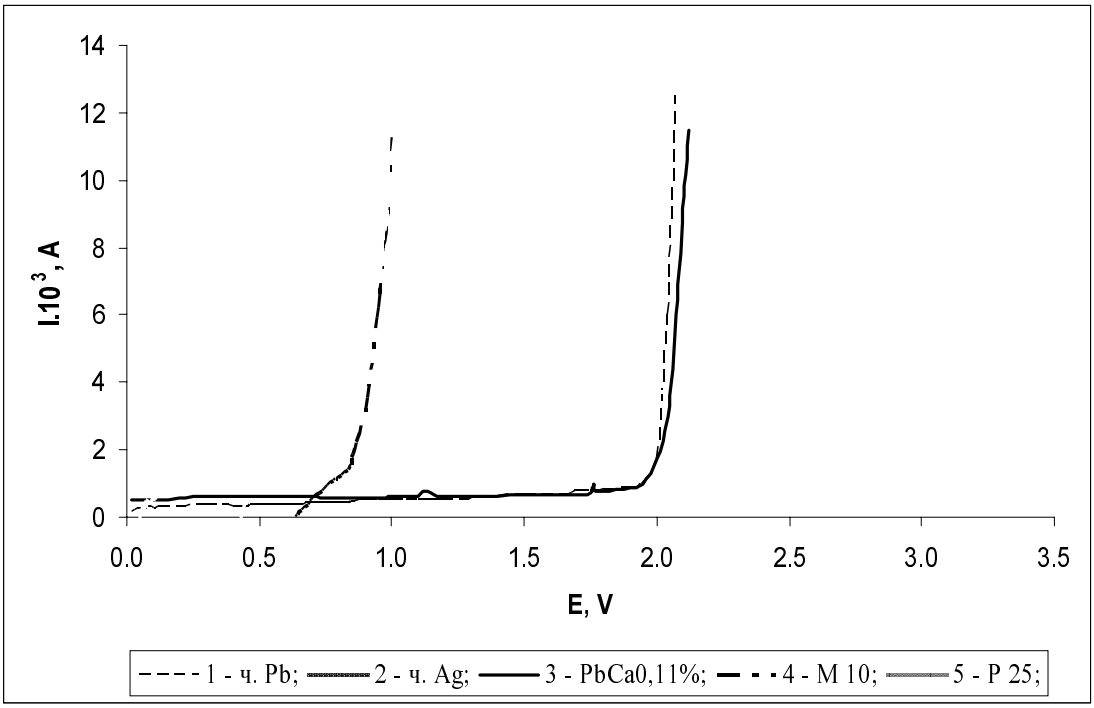

Figure 6. *Polarization dependencies of different anode materials, taken down at 20ºC in Chromispel – C, 250g.L^{-1} CrO_3, CrO_3:Cl^-=20:1*

The line of the curve of the polarization dependencies shows that pure silver is very quickly polarized, as well as polychrome acids influence it. The anode starts to destroy and these chemical and electrochemical interactions define the complex aspect of the polarization dependency.

Although slower, the anodes of lead and lead alloys also destroy. This typical chemical instability of theirs, as well as their high polarization make them unsuitable as anodes in *Chromispel – C*.

Out of the five different observed anode materials the most preferable one should be the metal ceramal alloy P 25, whose stability in *Chromispel – C* is almost equal to that of the platinum.

SUMMARY

- The total current distribution among separate anode reactions is determined.
- Potential dynamic curves are recorded under varying experimental conditions. The general course of platinum anode polarization curve and a mechanism of the anode process are proposed.
- The values of corrosion potential (E_c) and of potentials E_1 and E_2 as well the corresponding limiting currents I_1 and I_2 for the first and second step of polarization curve are determined.
- E_a is calculated according to the temperature-kinetic method and the nature of the electrode polarization was determined.

- The most suitable anodes to operate in *Chromispel – C* electrolytes appear to be Pt ones as well as anodes prepared from metal ceramal alloy P 25.

REFERENCES

1. Mantcheva, R., PhD thesis, BulgarianAcademy of Sciences, 1993.
2. Mantcheva R., I. Nenov, I. Gadschov, Metalloberfläche, 43, 6, 262-264, 1989.
3. Nenov I., R. Mantcheva, I. Gadschov, Metalloberfläche, 43, 7, 305-308, 1989.
4. Mantcheva R., I. Nenov, I. Gadschov, Metalloberfläche, 48, 2, 83-86, 1994.
5. Schluger, M.A., Galvanic coatings in machine building (in Russian), Moscow, "Mashinostroenie", vol. 1, 83, 1985.

ПЛОВДИВСКИ УНИВЕРСИТЕТ „ПАИСИЙ ХИЛЕНДАРСКИ“ – БЪЛГАРИЯ
НАУЧНИ ТРУДОВЕ, ТОМ 35, КН. 5, 2007 – ХИМИЯ
UNIVERSITY OF PLOVDIV „PAISII HILENDARSKI“ – BULGARIA
SCIENTIFIC PAPERS, VOL. 35, BOOK 5, 2007 – CHEMISTRY

PREDICTION OF BOILING POINTS OF ACYCLIC ALIPHATIC ALCOHOLS FROM THEIR STRUCTURE

Plamen Penchev, Nikolay Kochev, Vicktoria Vandeva, George Andreev
University of Plovdiv, Faculty of Chemistry,
Department of Analytical Chemistry

ABSTRACT

The normal boiling points for 120 C_5-C_8 aliphatic alcohols have been predicted using multiple linear regression analysis of different types of molecular descriptors derived from topology of the molecule and quantum chemistry calculations. Two new descriptors were introduced. The first one is the relative connectivity of oxygen atom expressed by the sum of all paths to the oxygen atom divided by Wiener index. The second one is a geometrical descriptor that reflects the oxygen atom shielding by spatially close atoms: it is a sum of the ratios of Van der Waals radius and distance from the oxygen to the corresponding atom raised to the third power.

Keywords: boiling point, multilinear regression, quantum chemistry, topology

INTRODUCTION

Boiling point (b.p.) is an important physicochemical property with practical value in chemistry, environmental protection and pharmaceutical industry. However, b.p. data often is not available, and therefore must be estimated theoretically. Estimation methods for b.p. have been widely explored [1-3] using topology of the molecule and/or quantum chemistry parameters calculated for optimized structure of the molecule.

Boiling point of a molecule depends on two major groups of factors. The first one includes intermolecular forces, such as dipole-dipole and Coulomb interactions. The second group accounts for the size and structure of the molecule as a whole, i.e. how the energy supplied by the heating is distributed into rotational and vibrational modes. That is why, every model for boiling point prediction has to account for these two trends with corresponding parameters.

In this work we present several approaches for theoretical calculation of normal boiling points of alcohols. The normal boiling points for 120 C_5-C_8 acyclic aliphatic alcohols have been predicted using multiple linear regression (MLR) analysis of different types of molecular descriptors: topological and quantum chemistry ones.

THEORETICAL MODELS

The topological parameters [4] used in different MLR models are given in Table 1. A new descriptor has been introduced designated as W^{O}_{Rel}. It is the relative connectivity of oxygen atom expressed by the sum of all paths to the oxygen atom divided by Wiener index.

Table 1. *Topological parameters used in the MLR models*

parameter	Parameter description
W	Wiener index – the sum of all path lengths in the molecule
W^{O}_{Rel}	The sum of all paths to the oxygen atoms divided by **W**
MW	Molecular weight
L_C	Size of the longest aliphatic chain
ξ	Molecular eccentricity index
$^{m}\chi$	Connectivity index of order m (m = 1)
$^{C}\chi$	Carbon connectivity - $^{1}\chi$ is calculated only for carbons
$^{m}\chi_c$,	Connectivity cluster index of order m (m = 3, 4)
$^{m}\chi_p$,	Connectivity path index of order m (m = 0, 1)
$^{m}\chi_{pc}$,	Connectivity path-cluster index of order m (m = 4, 5)
$^{m}\chi^{v}_{pc}$,	Valence connectivity path-cluster index of order m (m = 4, 5)
$BCUT_c$	The largest eigen value of the Burden matrix with weights based on partial charges
$^{m}\kappa$	Kier and Hall molecular shape indices of order m (m = 2)

The quantum chemistry calculations give the geometry of the molecule and some electronic parameters, such as dipole moment and partial charge of the atoms: the latter two determine the dipole-dipole and Coulomb interactions. For aliphatic acyclic alcohols it is the oxygen atom's charge that influences most the interaction. However, the strength of the interaction depends also on the oxygen surroundings which is quite different in various isomers of the alcohols. That is why, the new geometric parameter, so called oxygen shielding, O_{shield} , has been introduced.

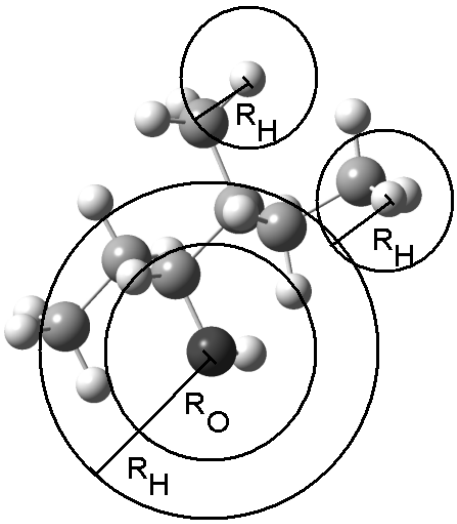

Figure 1. *Illustration of oxygen shielding*

O_{shield} is calculated by Equation (1) where the R_X is Van der Waals radius of the atom X and r_k is a distance of atom X_k (X = C or H) to the oxygen: see figure 1 for clarity.

$$O_{shield} = \Sigma (R_{Xk} / r_k)^3; \quad (1)$$

the sum is taken only for atoms $\mathbf{X_k}$ for which $\mathbf{r_k < R_O + R_H + R_{Xk}}$

The other quantum chemistry parameters tested in the models are the partial charge of the oxygen atom, q_O, partial charges of carbon, q_C, and hydrogen, q_H, that are connected to the oxygen and the dipole moment of the molecule, μ; it has to be pointed out that the partial charge is not a measurable quantity and depends on scheme for its calculation.

The set of all parameters or a selection of them was used for MLR calculations and significance of the parameters was determined by stepwise model selection.

RESULTS AND DISCUSSION

The three quantum chemistry parameters, O_{shield}, q_O, and q_C, showed high correlation with boiling point when alcohols are separated in classes (see Table 2). This has to be expected, as these parameters account for intermolecular interactions but not how the energy supplied by the heating is distributed. It has to be mentioned that the value of q_C depends entirely on the type of the alcohol (primary, secondary, tertiary) and is little influenced by the other substituents in the molecule but this is not the case with q_O which depends on all substituents. As can be seen from the table, q_H badly correlates with b.p. and the dipole moment shows weaker correlation than the first three parameters and also does not correlate with b.p. of the whole set.

On the other side, $^1\chi$ parameter has a good descriptive power of the whole set – its correlation coefficient with b.p.s is 0.883. This topological parameter accounts for both the branching of molecule and its size: the first one strongly correlates with the oxygen shielding.

Table 2. *The correlation coefficients between different parameters and b.p. calculated for different classes of isomers and for all alcohols*

parameter	pentanols	hexanols	heptanols	octanols	all alcohols
O_{shield}	-0.906	-0.928	-0.909	-0.820	-0.325
q_O	0.891	0.864	0.849	0.682	0.296
q_C	-0.816	-0.910	-0.851	-0.759	-0.389
q_H	0.222	0.521	-0.041	0.102	0.078
μ	0.867	0.696	0.615	0.727	0.262
$^1\chi$	0.848	0.794	0.758	0.717	0.883

Several different sets of descriptors were used in MRL model and a stepwise selection was performed upon them. The best seven descriptor sets are given in table 3.

Table 3. *Best descriptor sets obtained by different MLR stepwise selections*

Model #	Set of descriptors	Multiple R	Standard error (^{o}C)
1	ln(W)	0.861	9.24
2	ln(W), W^{O}_{Rel}	0.958	5.18
3	W^{O}_{Rel}, $(^{1}\chi)^{1/2}$	0.982	3.39
4	W^{O}_{Rel}, ln($^{1}\chi$), $^{4}\chi^{v}_{pc}$	0.986	2.98
5	W^{O}_{Rel} , ln($^{1}\chi$), $^{4}\chi^{v}_{pc}$, O_{shield}	0.975	2.88
6	ln(W), W^{O}_{Rel}, $^{0}\chi_{p}$, $^{1}\chi_{p}$, $^{5}\chi^{v}_{pc}$	0.990	2.54
7	ln(W), W^{O}_{Rel}, MW, $^{C}\chi$, $^{3}\chi_{c}$, $^{4}\chi_{c}$, $^{4}\chi_{pc}$, $^{4}\chi^{v}_{pc}$	0.992	2.34

The two-, three and five-variable models (#3, #4 and #6) showed less standard error than the models described in Jurs paper [1] with the same number of variables. On the other side, their other models performed better than ours. It is interesting that O_{shield} appeared only in the four-variable model (#5) and it is the only quantum chemistry parameter that competed with the topological ones. It is the only parameter in this study that depends on the 3-D structure of the molecule, and an adverse consequence of this fact is its variability upon conformational changes in the molecule. We intend to study this adverse effect in future work.

The eight-variable model (#7) is given with the following equation:

b.p. = (43.71±10.05) ln(W) + (134.04±17.96) W^{O}_{Rel} + (1.21±0.23) MW – (21.106.34) $^{C}\chi$ –(23.47±2.23) $^{3}\chi_{c}$ + (40.45±5.57) $^{4}\chi_{c}$ – (5.70±1.42) $^{4}\chi_{pc}$ + (10.91±1.81) $^{4}\chi^{v}_{pc}$ –(135.04±10.05)

USED SOFTWARE

The models based on topological descriptors were created with JBSMM (Java Based System for Molecular Modeling). It is an in-house developed software system [5] that supports the main stages of the molecular modeling: structure representation, descriptor calculation, MLR model creation and model statistics and validation. All quantum chemistry computations were carried out with the Gaussian 98W [A3] on level HF/6-31G(d) [6].

ACKNOWLEDGEMENTS

We would like to thank the Bulgarian National Fund for Scientific Research NFNI (project VUH-17/05) for supporting this scientific work.

REFERENCES

1. Smeeks, F.C. and Jurs, P.C. Prediction of boiling points of alcohols from molecular structure. Anal. Chim. Acta. 233, 111-119 (1990).
2. Katritzky, A.R.; Mu, L.; Lobanov, V. S.; Karelson, M. Correlation of Boiling Points with Molecular Structure. 1. A Training Set of 298 Diverse Organics and a Test Set of 9 Simple Inorganics. J. Phys. Chem. 100, 10400-10407 (1996).

3. Chunhui Lu; Weimin Guo; Yang Wang; Chunsheng Yin. Novel distance-based atom-type topological indices DAI for QSPR/QSAR studies of alcohols. J. Mol. Model. 12, 749–756 (2006)
4. Todeschini, R.; Consonni, V. Handbook of Molecular Descriptors; Wiley-VCH, 2000.
5. N. Kochev, O. Pukalov; Software system for molecular modeling – JBSMM; Balkan Conference of Young Scientists; 16-18 June, 2005, Plovdiv, Bulgaria.
6. Gaussian 98, Revision A.7, M. J. Frisch, G. W. Trucks, H. B. Schlegel, G. E. Scuseria, M. A. Robb, J. R. Cheeseman, V. G. Zakrzewski, J. A. Montgomery, Jr., R. E. Stratmann, J. C. Burant, S. Dapprich, J. M. Millam, A. D. Daniels, K. N. Kudin, M. C. Strain, O. Farkas, J. Tomasi, V. Barone, M. Cossi, R. Cammi, B. Mennucci, C. Pomelli, C. Adamo, S. Clifford, J. Ochterski, G. A. Petersson, P. Y. Ayala, Q. Cui, K. Morokuma, D. K. Malick, A. D. Rabuck, K. Raghavachari, J. B. Foresman, J. Cioslowski, J. V. Ortiz, A. G. Baboul, B. B. Stefanov, G. Liu, A. Liashenko, P. Piskorz, I. Komaromi, R. Gomperts, R. L. Martin, D. J. Fox, T. Keith, M. A. Al-Laham, C. Y. Peng, A. Nanayakkara, C. Gonzalez, M. Challacombe, P. M. W. Gill, B. Johnson, W. Chen, M. W. Wong, J. L. Andres, C. Gonzalez, M. Head-Gordon, E. S. Replogle, and J. A. Pople, Gaussian, Inc., Pittsburgh PA, 1998.

ПЛОВДИВСКИ УНИВЕРСИТЕТ „ПАИСИЙ ХИЛЕНДАРСКИ“ – БЪЛГАРИЯ
НАУЧНИ ТРУДОВЕ, ТОМ 35, КН. 5, 2007 – ХИМИЯ
UNIVERSITY OF PLOVDIV „PAISII HILENDARSKI“ – BULGARIA
SCIENTIFIC PAPERS, VOL. 35, BOOK 5, 2007 – CHEMISTRY

THE INVESTIGATION OF THE REACTION KINETICS OF o-PHENYLENEDIAMINE AND m-PHENYLENEDIAMINE IN THE PRESENCE Ag(I)

Özlen ALTUN*, Emre DÖLEN**
****Trakya University, Department of Chemistry, 22030 Edirne/TURKEY***
*****Marmara University, Department of Analytical Chemistry, 81010 Istanbul/TURKEY***
e-mail: ozlenaltun@yahoo.com

ABSTRACT

o- and m-phenylenediamines yield product through oxidative bonding in the presence of metals. Oxidative bonding products are azo dyes that are formed through a coloration reaction.

In this study, a visible spectrophotometric and differential methods have been developed for the reaction kinetics of o-phenylenediamine and m-phenylenediamine in the presence of Ag (I). Optimum conditions fort the reaction were established as pH=6 at λ=450 nm. When the oxidation of o-phenylenediamine and m-phenylenediamine by Ag (I) investigated, it was observed that in this reaction the following rate formula was found in this reaction:

$$V = k\,[Ag^{+}]^{0.5}\,[\text{o-phenylenediamine}]^{2}\,[\text{m-penylenediamine}]^{0.5}$$

The rate equation demonstrates that one molecule of m-phenylenediamine and four molecule o-phenylenediamine react with one molecule Ag (I).

Keywords: o-phebylenediamine, m-phenylenediamine, Spectrophotometry, Differential method, Reaction Kinetic

INTRODUCTION

The o-, m- and p- Phenylenediamines ($C_6H_4(NH_2)_2$), are the nitrogen analogs of the three dihydroxybenzenes ($C_6H_4(OH)_2$), pyrocatechol, resorcinol and hydroquinone, respectively; in fact, these hydroxy compounds are used as intermediates for the preparation of some of the phenylenediamines. These structural similarities have their counterpart in chemical reactivities. For instance, the ortho-

and para classes are very good reducing agents and used as antioxidants, while the meta compounds couple readily with diazotizedamines, forming useful dyes. Of the six possible tolylendiamines (toluendiamines or toluylendiamines), only one of the meta isomers and para isomer are commercial available [1].

The oxidation occurs quantitavely and proceeds in the presence of Cu(II) [2, 3], Ag(I) [4, 5]. Co(II) ions behaving as autooxidation catalysts. It is known that aromatic amines are suitable for the investigation. In the former study, 3,4-diaminobenzenesulfonic acid (DBS) [6, 7] was oxidised by the effect of catalytic Co(II) between a pH range of 7.4-8.4. The rate formula was found as follows:

$$V = k\,[Co^{+2}]\,[DBS]\,[O_2]$$

There is no reaction at pH < 7.4 and the reaction rate increases with the increasing pH. The oxidation product is 3,4-diiminobenzenesulfonic acid. The kinetics of these reactions related with o-phenylenediamine and m-phenylenediamine in the presence of Cu (II) were also investigated by using spectrophotometrical and differantial methods in this study.

In this study, the reactions related to o-phenylenediamine and m-phenylenediamine in the presence of Ag (I) [8] were investigated using spectrophotometric [9-15] and differential methods [16-18]. When the reactions of o-phenylenediamine and m-phenylenediamine in the presence of Ag (I) were investigated, it was observed that the following rate formula was found:

$$V = k\,[Ag^{+}]^{0.5}\,[\text{o-phenylenediamine}]^{2}\,[\text{m-penylenediamine}]^{0.5}$$

The result of the reactions between Ag (I) and o- and m-phenylenediamine mixtures it was found out that there is an oxidation by means of complexation. And as a result of oxidation, a diazo compound occured from amines and Ag (I) was reducted to elemental form.

EXPERIMENTAL

Investigation of the reaction conditions

Relative wideness of o-phenylenediamine was calculated from pH = 0 to 14 (K_1= 0.251, K_2 = $1.82x10^{-5}$) (Figure 1). During this investigation, o-phenylenediamine is taken as two protons (H_2A, α_0), and protons progrewing disappear in two steps. First proton disappears at the pH = 3 (HA^-, α_1), while second proton disappears at pH > 7 ($A^=$, α_2).

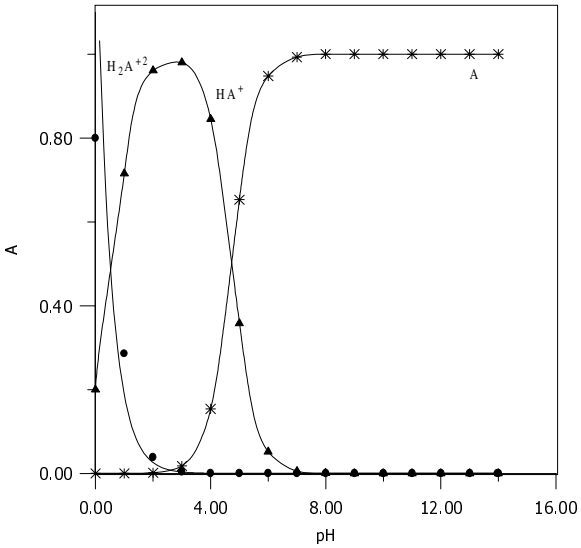

Figure 1. *Relative wideness of o-phenylenediamine*

o-Phenylenediamine exhibited an absorption at λ = 442nm at pH = 3 and it also showed an absorption λ = 424 nm at pH > 7.

Determination of the wavelength for the study

For determining the wavelength which would be used in the following reaction, various solutions including o-phenylenediamine, m-phenylenediamine and Ag (I) between pH = 5-10, were prepared in the proportion of 1:1:1 and the spectra were measured after waiting 10 minutes.

As a result of the investigation in various pH range, the oxidation product showed an absorption at λ = 450 nm and the absorbance was fixed after pH > 5. As a working medium, an absorbance value of λ = 450 nm and a pH value of 6 were chosen.

Dependence of the reaction rate to the Ag(I) concentration

A graphic of log v_o = f(log $[Ag^+]$) was drawn (Figure 2) related with the investigation of the effect of the Ag (I) concentration to the reaction rate which is related with the reaction of o- phenylenediamine and m-phenylenediamine by Ag (I). The equation obtained is log v_0 = -2.865 + 0.536log C. The straight line is $n_1 = 0.536 \approx 0.5$.

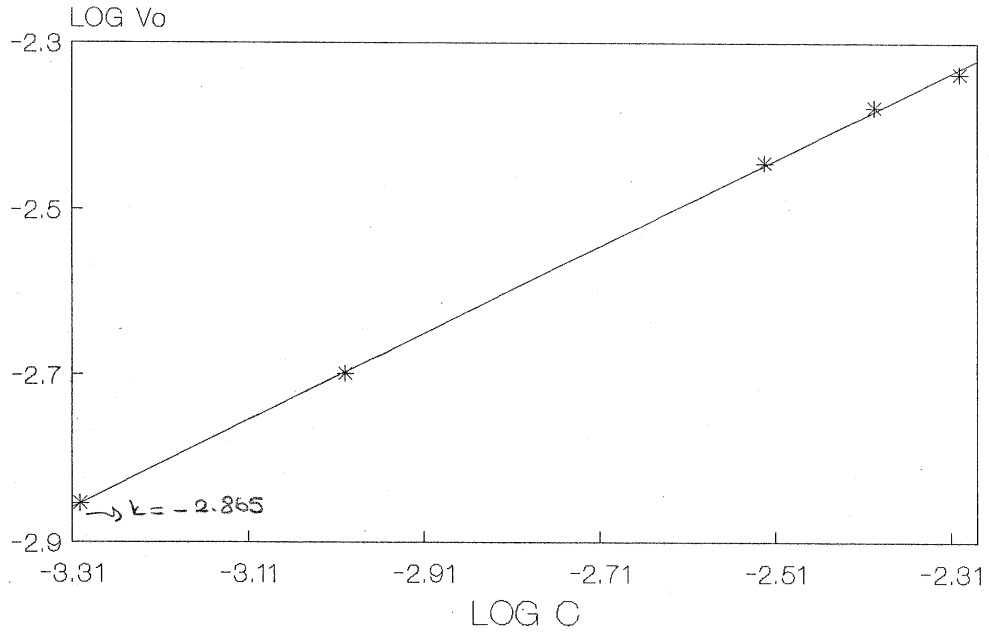

Figure 2. *λ = 450 nm, $C_{o\text{-}phen}$ = 1x10^{-3}M, $C_{m\text{-}phen}$ = 1x10^{-3}M, C_{Ag}^{+} = 0.5x10^{-3}- 5x10^{-3}M, pH = 6*

Dependence of the reaction rate to the o-phenylenediamine concentration

A graphic of log v_0 = f(log [o-phen]) was drawn (Figure 3) related with the investigation of the effect of the o-phenylenediamine concentration to the reaction rate which is related with the reaction of o-phenylenediamine and m-phenylenediamine by Ag (I). The equation obtained is log v_o = -2.900 + 1.977 log C. The straight line is n_2 = 1.9770 ≈2.

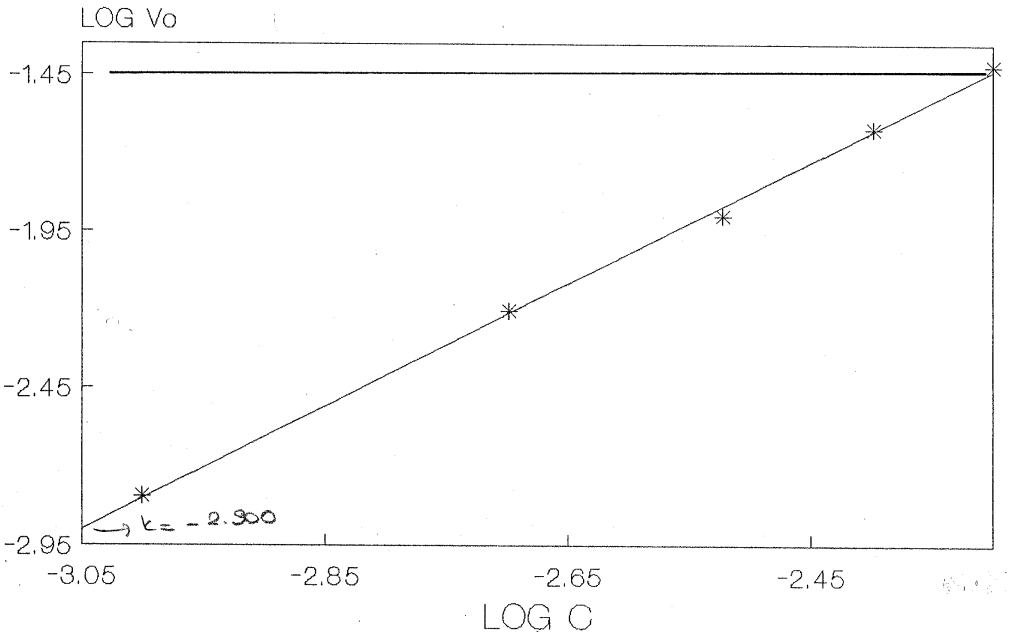

Figure 3. *λ = 450 nm, $C_{o\text{-}phen}$ = 1x10^{-3}- 5x10^{-3}M, $C_{m\text{-}phen}$ = 1x10^{-3}M, C_{Ag}^{+} = 1x10^{-3}M, pH = 6*

Dependence of the reaction rate to the m-phenylenediamine concentration

A graphic of log v_0 = f(log [m-phen]) was drawn (Figure 4) related with the investigation of the effect of the m-phenylenediamine concentration to the reaction rate which is related with the reaction of o-phenylenediamine and m-phenylenediamine by Ag (I). The equation obtained is log v_o = -2.730 + 0.5427 log C. The straight line is n_3= 0.5427 ≈0.5

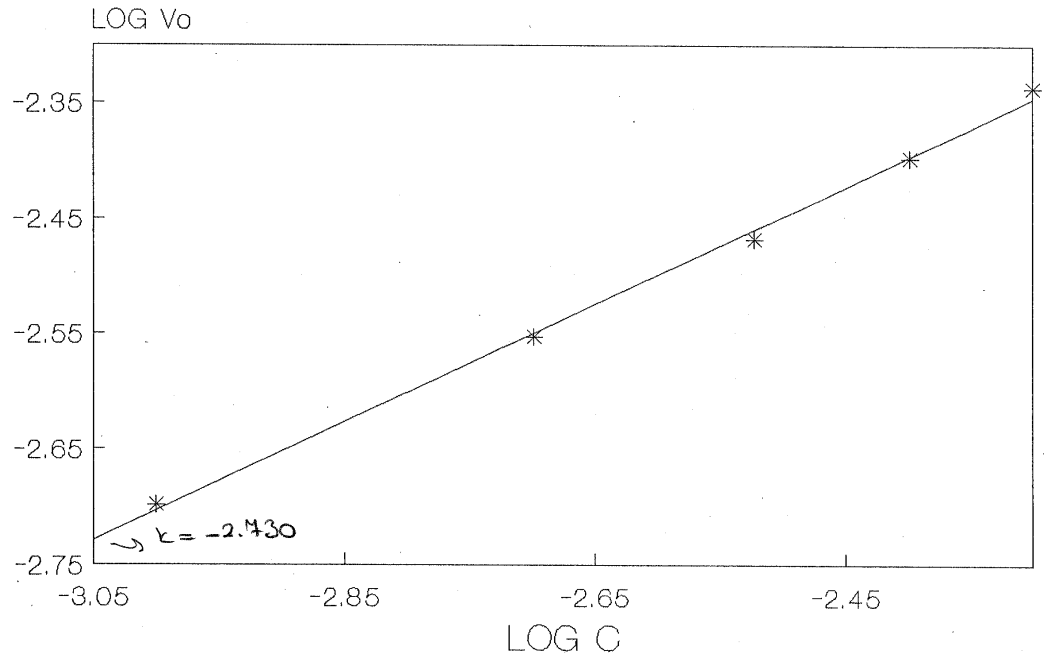

Figure 4. *λ = 450 nm, $C_{o\text{-}phen}$ = 1x10^{-3}M, $C_{m\text{-}phen}$ = 1x10^{-3}- 5x10^{-3}M, C_{Ag}^{+} = 1x10^{-3}M, pH = 6*

RESULTS

Following the investigation of the dependence of reaction rate Ag (I) concentration at pH = 6 the gradient was found as n_1 = 0.5 (Figure 2). However, in the investigation of the dependence reaction rate to o-phenylenediamine concentration the gradient was found as n_2 = 2 (Figure 3) and the dependence reaction rate to m-phenylenediamine concentration the gradient was found as n_3 = 0.5 (Figure 4) .

Considering this, the rate equation related with the oxidation of o-phenylenediamine and m-phenylenediamine by Ag (I), is found as the following equation ie.

$$V = k\,[Ag^{+}]^{0.5}\,[\text{o-phenylenediamine}]^{2}\,[\text{m-penylenediamine}]^{0.5}$$

The rate equation demonstrates that one molecule of m-phenylenediamine and four molecule o-phenylenediamine react with one molecule Ag (I).

REFERENCES

1. Kirk Othmer, Encylopedia of Chemical Tech., Intesinc Published, New York, 1966, 482, 378, 380-384, 687.
2. T. A. Wright, Metals and Alloys,1932, 246, 3.
3. W. Adolphi, Chemiker, 1928, 109, 52
4. K. H. Saunders., The Aromatic Diazo Compounds, London, 1949, 21-22-329.
5. Holzach, K., Die Aromatischen Diazoverbindungen, Studgard, 1947, 20-26, 246-253.
6. K. Wutrich, Fallab, S., Helv. Chim. Acta, 1964, 1440-1448, 47.
7. K. Wutrich, Fallab, S., Helv. Chim. Acta, 1964, 1609-1616, 47.
8. E.P. Shkrobot, N.I. Shebarshina, Nauch. Issled. Inst. Tsvet. Metal, 1971, 34, 7-22.
9. R. L. Robertus, V. Levin, Anal. Chem., 1968, 2053-2054, 40.
10. J. Lieberman, K. J. Yun, Chem. Educ., 1988, 728-729, 65.
11. B. W. Budesinsky, Svec, J.J., Anal. Chim. Acta, 1971, 115-124, 55.
12. E. Özcan, C. Bayat, Chim. Acta Turc.,1980, 195-210, 8.
13. B. Ülküseven, E. Özcan, Chim. Acta Turc., 1986, 13-21, 14.
14. Mori, H. Tominaga, Y. Fujita, Analytical Letters, 1997, 30 (5), 953-961.
15. Y. Fujita, .I. Mori, T. Matsuo, Analytical Sciences, 1999, 15, 1009-1012.
16. J. H. Van't Hoff, Etudes de Dynamique Chimique, Amsterdam, 1988, 87.
17. M. Letort, J. Chim. Phys., 1937, 206, 34.
18. B. Anılanmert, G. Yalçın, F. Arıöz and E. Dölen, *Analytical Letters,* 200134, 113-123.

ПЛОВДИВСКИ УНИВЕРСИТЕТ „ПАИСИЙ ХИЛЕНДАРСКИ“ – БЪЛГАРИЯ
НАУЧНИ ТРУДОВЕ, ТОМ 35, КН. 5, 2007 – ХИМИЯ
UNIVERSITY OF PLOVDIV „PAISII HILENDARSKI“ – BULGARIA
SCIENTIFIC PAPERS, VOL. 35, BOOK 5, 2007 – CHEMISTRY

TEMPLATE SYNTHESIS OF NEW SCHIFF-BASE COMPLEXES AND DETERMINATION OF THE STRUCTURE OF THESE COMPLEXES

ULUÇAM Gühergül, BEYNEK Nesrin
Trakya University, Faculty of Art and Science, Department of Chemistry, 22030, Edirne, Türkiye

ABSTRACT

In this study, two new Zn(II) and Cd(II) acyclic Schiff-base complexes, $[Zn(\mathbf{L})](ClO_4)_2$ and $[Cd(\mathbf{L})](ClO_4)_2$, have been prepared via templated [1+2] condensation of 6,6'-*bis*(2-aminothiophenoxymethyl)-2,2'-bipyridine with 2-furaldehyde. The structure of these complexes was elucidated by using spectroscopic methods.

Keywords: Schiff-base, template synthesis, Cd(II) and Zn(II) complexes.

INTRODUCTION

Schiff-base complexes recently have taken more attention in bioinorganic and biochemistry in medicine because of the fact that it has antimicrobial and chemotherapy features.[1,2] The potential biological activity of complexes containing sulfur and nitrogen may be reason for this increased interest. In particular complexes with N and/or S donor ligands of copper(II),[3,4] cobalt(II),[5] nickel(II),[3,5] platinum(II)[1,3,6] and iron(II/III)[6] are known sometimes to act as antitumor or therapeutic agents. Many efforts have been made to establish further metal-containing cytostatics however, without great success. Only little is known about the antitumor efficacy of some transition metals such as zinc(II),[7] and cadmium(II). For this reason, we synthesized two new $N_4S_2O_2$ Schiff base complexes of these transition metals. Recently we also synthesized and characterized some new similar macrocyclic and acyclic Schiff base complexes using these metals.[8-10]

In this study, in the presence of cadmium(II) and zinc(II) perchlorate salts that control the reaction, by using 6,6´-*bis*(2-aminothiophenoxymethyl)-2,2´-bipyridine and 2-furaldehyde, open chain $N_4S_2O_2$ donor complexes were synthesized. The structure of these complexes were elucidated by using spectroscopic methods.

EXPERIMENTAL

Enstrumentation

Melting points were determined using an Gallenkamp MPD350.BM2.5 digital melting point apparatus and were uncorrected. The compounds were checked for purity by TLC on silica gel 60 F_{254} (Merck). Elemental analyses were performed on a CHNS-O Carlo Erba EA 1108 elemental analyser; IR spectra were obtained with a Shimadzu 470 IR spectrophotometer using nujol mulls or KBr disc; ^{1}H NMR spectra were recorded with a Varian (300 MHz) or Bruker spectrometer (250 MHz) in $CDCl_3$ as solvent. ^{13}C NMR spectra were recorded with a Varian (75.5 MHz) in $CDCl_3$ as solvent; MS-FAB$^+$ spectra were obtained with a Finnigan Mat 95 mass spectrometer. ESI MS spectra were recorded on a Finnigan LCQ mass spectrometer.

Materials

THF was distilled from sodium metal in the presence of benzophenone immediately prior to use. 1,4-Dioxane was distilled prior to use. Et_4NI was dried at 100 ºC under reduced pressure. Zinc dust was washed with successive portions of dilute hydrochloric acid, distilled water, ethanol, acetone and diethyl ether immediately prior to use to remove the oxide layer. All other chemicals and solvents were of reagent grade and used as commercially purchased without further purification. Preparation of $NiCl_2(PPh_3)_2$ was followed to literature method.[11] 6-Bromo-2-methylpyridine and 6,6'-*bis*(bromomethyl)-2,2'-bipyridine were prepared according to literature procedures. [12,13] 6,6'- dimethyl-2,2'-bipyridine was prepared by a slight modification of the method of Iyoda *et. al.* [14]

Preparation of 6,6'-Bis(2-aminothiophenoxymethyl)-2,2'-bipyridine [10]

Solution of sodium ethoxide (2.30 g sodium, 0.10 mol ; absolute ethanol 150 mL) were added to solution of 2-aminothiophenol (12.5 g, 0.10 mol) in absolute ethanol (150 mL) at room temperature, under argon gas. Then 6,6'-*bis*(bromomethyl)-2,2'-bipyridine (17.10 g, 0.05 mol) in absolute ethanol (100 mL) was added and the reaction mixture refluxed for 4 h. On cooling, the reaction mixture was poured into water (400 mL). The product (cream colour) was collected by filtration, washed with water and dried (yield 89 %). m.p. 97-99 ºC.

$\gamma_{max/cm-1}$ **(KBr disc):** 3440-3328 (N-H); 1603, 1561 (aromatic ring).

δ_H **(300 MHz; $CDCl_3$):** 4.14 (4H, s, CH_2), 4.38 (4H, s, NH_2), 6.61 (2H, t, *J* 7.5 Hz), 6.70 (2H, d, *J* 8.2 Hz), 7.03 (2H, d, *J* 7.6 Hz), 7.09 (2H, t, *J* 7.5 Hz), 7.26 (2H, d, *J* 5.3 Hz), 7.66 (2H, t, *J* 7.8 Hz), 8.18 (2H, d, *J* 7.9 Hz).

δ_C **(75.5 MHz; $CDCl_3$):** 41.22 (CH_2), 115.28, 117.33 (C), 118.76, 120.23, 123.54, 130.42, 136.85, 137.79, 148.72(C), 155.31 (C), 157.55 (C).

m/z 431 [(M+H)$^+$, 100 %]; **$C_{24}H_{22}N_4S_2$ calculated :** C 66.9 %, H 5.2 %, N 13.0 %, S 14.9 % **found :** C 66.7 %, H 5.2 %, N 13.0 %, S 15.3 %.

Metal-ion Controlled Synthesis of L Complexes in the Presence of Zn(II) and Cd(II) perchlorate salts.

The complexes of **L** were obtained from [1+2] Schiff-base condensations of 6,6'-*bis*(2-aminothiophenoxymethyl)-2,2'-bipyridine and 2-furaldehyde in methanol in the presence of Zn(II) and Cd(II) perchlorate salt (Scheme 1). The yields, colours and API-ES mass (m/z) spectral data and IR data of the complexes are given respectively in Table 1 and Table 2.

Table 1. *Colours, yields and the API-ES mass spectrum for the complexes*

Complex	Colour of complex	% yield	Peak (m/z)	Assingment
$[Zn(\mathbf{L})](ClO_4)_2$	light brown	80	749.0 650.95 587.10 325	$[Zn(\mathbf{L})(ClO_4)]^+$ $[Zn\mathbf{L}]^{2+}$ $[\mathbf{L}+H]^+$ $½[Zn\mathbf{L}]^{2+}$
$[Cd(\mathbf{L})](ClO_4)_2$	light brown	40	796.90 697.95 587.10 349.9	$[Cd(\mathbf{L})(ClO_4)]^+$ $[Cd\mathbf{L}]^{2+}$ $[\mathbf{L}+H]^+$ $½ [Cd\mathbf{L}]^{2+}$

Table 2. *Infrared (KBr/disc) spectral data for the complexes*

Complex	ν[C=N]	pyridine	ν(anion)
$[Zn(\mathbf{L})](ClO_4)_2$	1612	1596	1094, 624
$[Cd(\mathbf{L})](ClO_4)_2$	1612	1596	1094, 624

RESULTS AND DISCUSSION

All the complexes were prepared by a template synthesis, in which the Schiff base macrocyclic ligand resulted from the condensation of 6,6'-*bis*(2-aminothiophenoxymethyl)-2,2'-bipyridine with 2-furaldehyde in methanol in the presence of Zn(II) and Cd(II) perchlorate salt (Scheme 1). For the synthesis of diamine compound, 6,6'-*bis*(2-aminothiophenoxymethyl)-2,2'-bipyridine, 6-amino-2-methylpyridine was brominated with concentrated aqueous hydrobromic acid and bromine.[12] Then 6,6'-dimethyl-2,2'-bipyridine was prepared using 6-bromo-2-methylpyridine by a modification of the method described by Iyoda *et. al*. [14] and it was reacted with 47 % hydrobromic acid.[13] Then, one equivalent of 6,6'-*bis*(bromomethyl)-2,2'-bipyridine was reacted with two equivalents of 2-aminothiophenol in ethanol under an inert atmosphere. Physical data for all compounds are given in the Experimental Section.

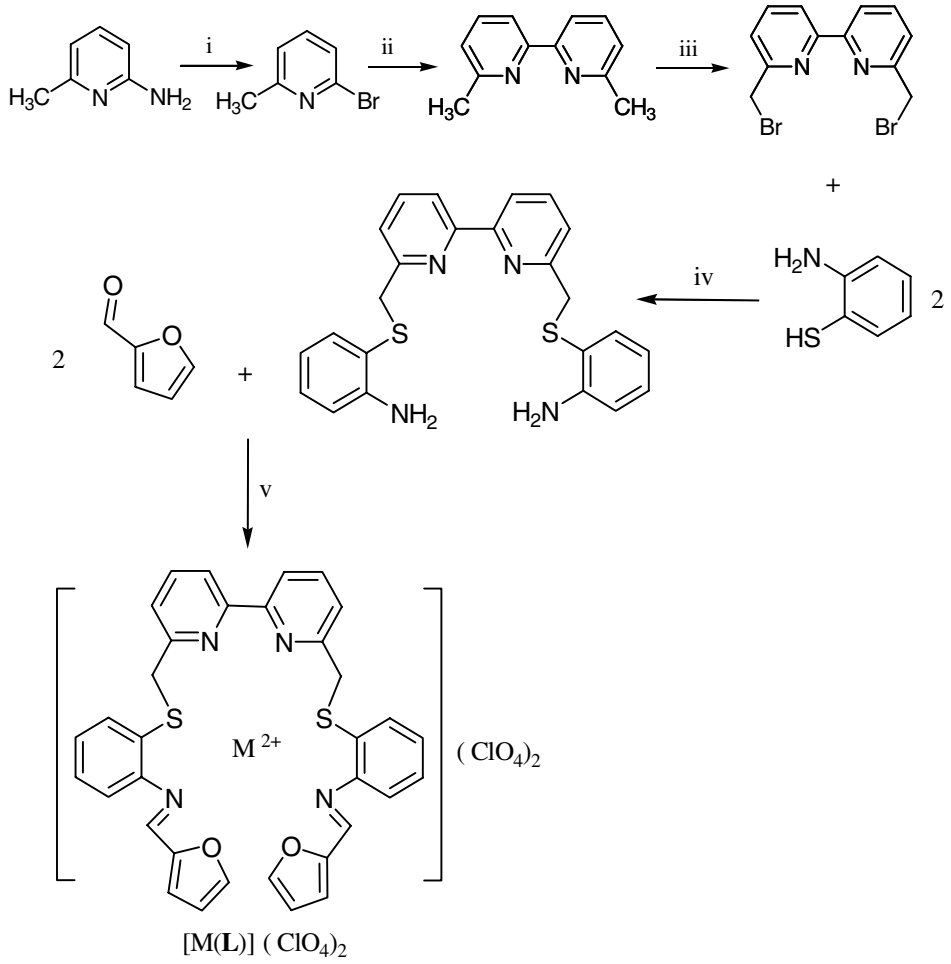

Scheme 1. *Synthetic route to [ML](ClO₄)₂.*
***i**: %47 HBr, Br₂, NaNO₂ then NaOH, **ii**: NiCl₂(PPh₃)₂, Zn, Et₄NI, THF under argon gas, **iii**: CCl₄, NBS then benzoyl peroxide, **iv:** Na, EtOH under argon gas, **v:** MeOH, [M(ClO₄)₂] (M=Zn²⁺, Cd²⁺).*

The complexes were obtained with 40-80 % yields. The infrared spectra of these metal complexes in the region 400-4000 cm^{-1} show a strong absorption band at 1612 cm^{-1}, which assigned to the C=N streching vibration, indicating the formation of the Schiff base products. Furthermore, the absence of C=O and N-H streching vibrations in the spectra of the complexes, as compared to the aldehyde and diamine, respectively. For the metal complexes absorbtions at 1094 and 624 cm^{-1} were assigned to the ν_3 and ν_4 streching modes of ionic perchlorate.[15]

The API-ES mass spectrum of the complex, Zn(**L**)$(ClO_4)_2$ and Cd(**L**)$(ClO_4)_2$ in positive ion mode is structurally enlightening, since it displays a series of intermediate breakdown species. The loss of an anionic perchlorate ion from the neutral parent molecule generates the cationic $[Zn(\mathbf{L})(ClO_4)]^+$ and $[Cd(\mathbf{L})(ClO_4)]^+$, which is the first peak observed at respectively m/z 749.0 and 796.90 in the mass spectra. The loss of a second perchlorate anion occurs to generate $[Zn\mathbf{L}]^{2+}$ at m/z 650.95 and $[Cd\mathbf{L}]^{2+}$ at m/z 697.95. The loss of counterion for these complexes is also accompanied by the presence of the free ligand at m/z 587.10 for $[\mathbf{L}+H]^+$ in the mass spectrum.

REFERENCES

1. H. M. Pinedo and J.M. Schornagel, Platinum and Other Metal Coordination Compounds in Cancer Chemotherapy 2*,* (Plenum Press, New York, 1996).
2. N. Beynek, G. Uluçam, B.A. Tüylü, K. Benkli, H. Zeytinoğlu*, Drug and Chemical Toxicology*, 2007, 30;4, 399-410 .
3. Z. Afrasiabi, E. Sinn, J. Chen, Y. Ma, A.L. Rheingold, L.N. Zakharov, N. Rath and S. Padhye, *Inorg. Chim. Acta*, 357, 271-78 (2004).
4. F. Liang, C. Wu, H. Lin, T. Li, D. Gao, Z. Li, J. Wei, C. Zheng and M. Sun, *Bioorg. & Med. Chem. Lett.,* 13, 2469-72 (2003).
5. P. Kamalakannan and D. Venkappayya, *J. Inorg. Biochem.,* 90, 22-37 (2002).
6. J. Patole, S. Padhye, M.S. Moodbidri and N. Shirsat, *Eur. J. Med. Chem.,* 40, 1052-55 (2005).
7. D. Kovala-Demertzi, P.N. Yadav, J. Wiecek, S. Soulika, T. Varadinova, and M.A. Demertzis, *J. Inorg. Biochem.,* 100, 1558-67 (2006).
8. N. Beynek, M. McPartlin, B.P. Murphy and I.J. Scowen, *Polyhedron,* 17, 2137 (1998).
9. T. Adatia, N. Beynek and B.P. Murphy, *Polyhedron,* 14, 335 (1995).
10. N. Beynek, PhD. Thesis, University of Manchester (UMIST), Manchester, (1997).
11. L. M. Venanzi, *J. Chem. Soc.,* 2, 719-724 (1958).
12. R. Adams and S. Mıyano, *J. Am. Chem. Soc.,* 76, 3168-3171 (1954).
13. J. C. Rodriguez-Ubis, B. Alpha, D. Plancherel, J. M. Lehn, *Helv. Chim. Acta*., 1984, 67, 8, 2264-2269.
14. M. Iyoda, H. Otsuka, K. Sato, N. Nısato, M. Oda, *Bull. Chem. Soc. Jpn*., 1990, 63, 80.
15. K. Nakamoto, Infrared and Raman Spectra of Inorganic and Coordination Compounds, John Wiley, New York, 1972, 3rd ed.

ПЛОВДИВСКИ УНИВЕРСИТЕТ „ПАИСИЙ ХИЛЕНДАРСКИ“ – БЪЛГАРИЯ
НАУЧНИ ТРУДОВЕ, ТОМ 35, КН. 5, 2007 – ХИМИЯ
UNIVERSITY OF PLOVDIV „PAISII HILENDARSKI“ – BULGARIA
SCIENTIFIC PAPERS, VOL. 35, BOOK 5, 2007 – CHEMISTRY

OPTIMIZATION OF OPERATIONAL CONDITIONS OF ETHANOL EXTRACTION OF ROSMARINIC ACID FROM LEMON BALM *(Melissa officinalis L.)*

G. Angelov[1], P. Penchev[1], J.-S. Condoret[2]
[1] Institute of Chemical Engineering, Bulgarian Academy of Sciences, Acad. Bonchev St., bl. 103, 1113 Sofia, Bulgaria, e-mail: p.i.penchev@abv.bg
[2] Laboratory of Chemical Engineering, CNRS, 5 rue Paulin Talabot, 31106 Toulouse, France

ABSTRACT

The process of ethanol extraction of a substance with antioxidant properties, rosmarinic acid (RA), from the plant Lemon balm *(Melissa officinalis L.)* is studied. The impact of some main process parameters (solvent concentration, process temperature and process duration) is experimentally determined, and the results helpful for process optimization are obtained. The general conditions for better practical extraction of RA from Lemon balm are defined.

Keywords: extraction, rosmarinic acid, Lemon balm

INTRODUCTION

Bioactive components are largely used in pharmacy, cosmetics, and perfumery or as nutritional additives. Substances of natural origin are preferred as substitutes of synthetic chemicals in order to reduce allergies and side effects. Consequently, studies on isolation of natural bioactive substances from plants contribute to development of processes with practical application.

Lemon balm *(Melissa officinalis L.)* has multiple positive actions on the human health due to its contents of natural bioactive substances [1-5]. This plant contains significant amounts of antioxidants (flavonoids, polyphenols) with main active component rosmarinic acid (RA) [1-4, 6].

Previous studies apply different kinds of treatment of Lemon balm with aim to isolate RA for studying its antioxidant activity, for comparison of its content in different plants, or for validation of different analytical methods [1, 3, 4, 6-11].

In this study, an experimental determination of optimized conditions for extraction of rosmarinic acid from Lemon balm is presented aimed at development of a practical process for production of RA using a harmless solvent ethanol.

MATERIALS AND METHODS

Rosmarinic acid has been chosen as a target component accounting for its recognized bioactive properties [7, 8, 12-15]. The choice of Lemon balm as raw material is due to its high content of rosmarinic acid and also to the fact that the plant is widely spread in nature and easy for cultivation [1, 3, 6-11]. Ethanol is chosen because of its frequent use as a harmless solvent for pharmacological and other applications. The goal of this study is to determine the process conditions, at which maximal amount of RA can be extracted from the raw material using ethanol as a solvent.

Solid - liquid extraction process has been used for isolation of RA from Lemon balm. Essentially, it consists of bringing together the raw material with the solvent, which dissolves the desired compound from the solid. All experiments have been made with dry plant at batch conditions. A weighted amount of dried and ground Lemon balm has been put in a glass flask. In order to operate at unsaturated concentrations, a measured amount of solvent has been added in large excess, and the flask has been continuously agitated for 24 hours in a thermostatic agitator. The samples withdrawn from the liquid phase have been filtered through a 20 μm micro-filter for elimination of solid particles prior to the injection into the analytical device (HPLC chromatograph).

Analytical method

RA concentration of the samples has been determined by means of high performance liquid chromatography (HPLC) with UV detector. Calibration solutions of RA in methanol have been prepared starting from pure RA (Fluka, purum > 95 %). A column Discovery® C18 (25cm X 4.6 mm, 5μ), Supelco has been used. The mobile phase has been methanol-water mixture 80:20 (v:v) with pH fixed at 2.5 using formic acid. The flow rate has been 0.4 ml/min and injection volume - 20 μl. All analyses have been carried out at ambient temperature. UV spectrum for the analysis of RA has been fixed at 280 nm [1, 11].

RESULTS AND DISCUSSION

The extraction yield w has been expressed as mass output, calculated by the following relation:

$$w(\%) = \frac{m_{ex}}{m_{rm}}.100$$

where m_{ex} is the extracted mass of RA in the sample calculated by the chromatographic analysis results, and m_{rm} is mass of the raw material.

Influence of solvent concentration

In order to determine the influence of solvent concentration, water solutions with various contents of ethanol have been used as solvents. The results are illustrated on Fig. 1.

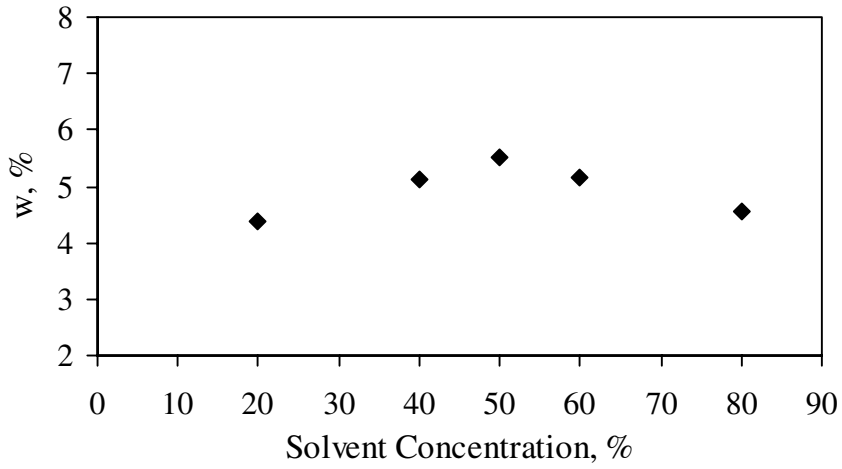

Figure 1. *Influence of solvent concentration on extraction yield*

Optimal yield has been obtained with ethanol diluted with water to 50 %. This result is clearly manifested by a distinct maximum at this value. The lower yield of more concentrated solutions can be explained by the increased solubility of other substances (chlorophyll and others) in concentrated alcohol, which engage the extraction capacity of the solvent.

Influence of temperature

The extraction process has been carried out at optimal solvent concentration and various temperatures taken in an interval from room temperature to temperatures below the solvents boiling point. The results are plotted on Fig. 2 and show a tendency for positive impact of increased temperature.

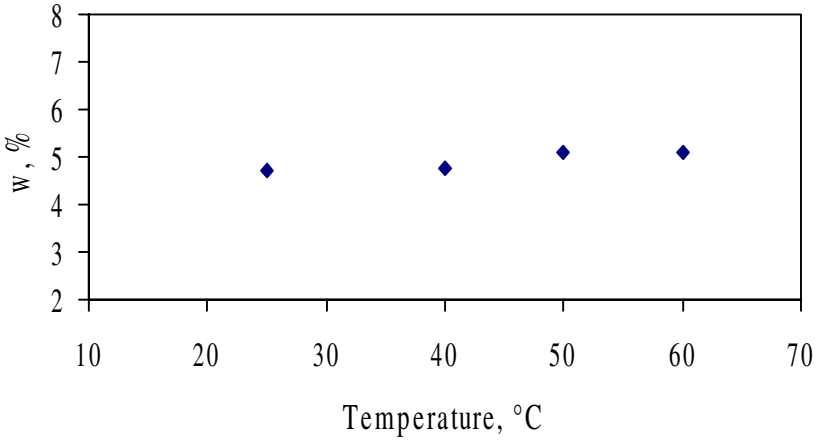

Figure 2. *Influence of temperature on extraction yield*

However, it is seen that the yield does not vary significantly in the studied temperature interval, with particularly small change between 50 and 60°C.

Consequently, it is to recommend choosing operation at lower temperature (for example about 50°C), because such a regime will be with lower energy consumption and reduced risks for thermal destruction of the extracted substance.

Kinetic study

This study has been made in order to determine the development of the extraction process in the course of time. Samples at different moments of process duration have been taken and analyzed. Fig. 3 illustrates the results.

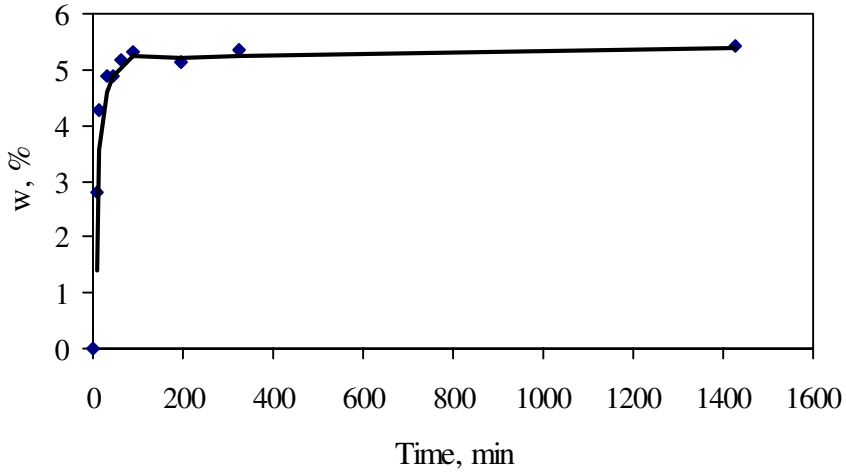

Figure 3. *Extraction yield in the course of time*

Two periods with different kinetic mechanisms might be clearly identified. Initially, the process velocity is high, which results in fast increase of RA concentration. After some time the mass transfer rate becomes slower, and the curve becomes nearly parallel to the abscissa, indicating negligible further concentration changes.

During the first period of fast mass transfer, the majority of the target substance is extracted. Consequently, the kinetic curve can serve to determine the process duration, which in this case is about 90 min.

CONCLUSION

An experimental study on ethanol extraction of rosmarinic acid from Lemon balm is carried out. The main operational conditions are varied in order to determine their impact on the process efficiency. As a result, the optimal solvent concentration, suitable process temperature, and duration of the process of extraction of rosmarinic acid from Lemon balm are determined.

ACKNOWLEDGEMENT

The partial financial support of the Bulgarian Council for Scientific Research is gratefully acknowledged.

REFERENCES

1. Caniova A., Brandsteterova E., HPLC Analysis of Phenolic Acids in Melissa Officinalis, J. Liq. Chrom. & Rel. Technol., 24, 17, 2647 (2001).
2. Ribeiro M.A., Bernardo-Gil M. G., Esquivel M. M., Melissa officinalis, L.: study of antioxidant activity in supercritical residues, Journ. of Supercritical Fluids, 21, 51 (2001).
3. Tóth J. Mrlianova, M., Tekelova, D., Korenova M., Rosmarinic acid – an important phenolic active compound of Lemon balm (Melissa officinalis L.), Acta Facultalis Pharmaceuticae Universitatis Comenianae, Tomus L, 139 (2003).
4. Ziakova A., Brandsteterova E., Blahova E., Matrix solid-phase dispersion for the liquid chromatographic determination of phenolic acids in Melissa officinalis, Journ. of Chromatography A, 983, 271 (2003).
5. Herodez S., Hadolin M., Skerget M., Knez Z., Solvent extraction study of antioxidants from Balm *(Melissa officinalis L.)* leaves, Food Chemistry, 80, 275 (2003).
6. Janicsak G., Mathe I., Miklossy-Vari V., Blunden G., Comparative studies of the rosmarinic and caffeic acid contents of Lamiaceae species, Biochemical Systematics and Ecology, 27, 733 (1999).
7. Lamaison J. L., Petitjean-Freytet C., Carnat A., Rosmarinic acid, total hydroxycinnamic derivatives and antioxidant activity of Apiaceae, Borraginaceae and Lamiceae medicinals, Ann. Pharm. Fr., 48(2), 103 (1990).
8. Lamaison J. L., Petitjean-Freytet C., Carnat A., Medicinal Lamiaceae with antioxidant properties, a potential source of rosmarinic acid, Pharm. Acta Helv., 66(7), 185 (1991).
9. Zgorka G., Glowniak K., Variation of free phenolic adcid in medicinal plants belonging to the Lamiaceae family, J. of Pharmaceutical and Biomedical Analysis, 26, 79 (2001).
10. Wang H., Provan G. J., Helliwell K., Determination of rosmarinic acid and cafeic acid in aromatic herbs by HPLC, Food Chemistry, 87, 307 (2004).
11. Boyadzhiev L., Dimitrova V., Extraction and Liquid Membrane Preconcentration of Rosmarinic Acid from Lemon Balm (Melissa Officinalis L.), Sep. Sci. and Technology, 41, 877 (2006).
12. Lopez-Arnaldos T., Lopez-Serrano M., Barcelo A., Calderon A. A., Zapata M., Spectrophotometric determination of rosmarinic acid in plant cell cultures by complexation whit Fe^{+} ions, Fresenius J. Anal. Chem., 351, 311 (1995).
13. Janicsac G., Mathe I., Parallel Determination of Rosmarinic and Caffeic Acids by TLC densitometry, Chromatographia, 46, 322 (1997).
14. Wang M., Li J., Rangarajan M., Shao Y., LaVoie E. J., Haung T. C., Ho C. T., Antioxidative Phenolic Compounds from Sage (Salvia officinalis), J. Agric. Food Chem., 46, 4869 (1998).
15. Zelic B., Hadolin M., Bauman D., Vasic-Racki D., Recovery and Purification of Rosmarinic Acid from Rosemary Using Electrodialysis, Acta Chim. Slov., 52, 126 (2005).